



Molecular basis of the interaction of novel tributyltin(IV) 2/4-[(E)-2-(aryl)-1-diazenyl] benzoates endowed with an improved cytotoxic profile: Synthesis, structure, biological efficacy and QSAR studies

Tushar S. Basu Baul^{a,*}, Anup Paul^a, Lorenzo Pellerito^b, Michelangelo Scopelliti^b, Claudia Pellerito^b, Palwinder Singh^c, Pooja Verma^c, Andrew Duthie^d, Dick de Vos^e, Rajeshwar P. Verma^f, Ulli Englert^g

^a Department of Chemistry, North-Eastern Hill University, NEHU Permanent Campus, Umshing, Shillong 793 022, India

^b Dipartimento di Chimica Inorganica e Analitica "Stanislao Cannizzaro" Università degli Studi di Palermo, Viale delle Scienze, Parco D'Orleans II, Edificio 17, 90128 Palermo, Italy

^c Department of Chemistry, Guru Nanak Dev University, Amritsar 143005, India

^d School of Life and Environmental Science, Deakin University, Geelong Victoria 3217 Australia

^e Pharmachemie BV, PO Box 552, 2003 RN Haarlem, The Netherlands

^f Department of Chemistry, Pomona College, 645 North College Avenue, Claremont, California 91711, USA

^g Institut für Anorganische Chemie, RWTH Aachen University, 52056 Aachen, Germany

ARTICLE INFO

Article history:

Received 10 March 2010

Received in revised form 2 May 2010

Accepted 3 May 2010

Available online 10 May 2010

Keywords:

Tributyltin(IV) compounds

Arylazobenzoate

Spectroscopy

X-ray crystallography

Cell lines

Anti-cancer drugs

Hydrophobicity

QSAR

Docking studies

ABSTRACT

A series of tributyltin(IV) complexes based on 2/4-[(E)-2-(aryl)-1-diazenyl]benzoate ligands was synthesized, wherein the position of the carboxylate and aryl substituents (methyl, *tert*-butyl and hydroxyl) varies. The complexes, Bu₃SnL^{1–4}H (1–4), have been structurally characterized by elemental analysis and IR, NMR (¹H, ¹³C, and ¹¹⁹Sn) and ¹¹⁹Sn Mössbauer spectroscopy. All have a tetrahedral geometry in solution and a trigonal bipyramidal geometry in the solid-state, except for Bu₃SnL⁴H (4) that was ascertained to have tetrahedral coordination by X-ray crystallography. Cytotoxicity studies were carried out on human tumor cell lines A498 (renal cancer), EVSA-T (mammary cancer), H226 (non-small-cell lung cancer), IGROV (ovarian cancer), M19 MEL (melanoma), MCF-7 (mammary cancer) and WIDR (colon cancer). Compared to cisplatin, test compounds 1–4 had remarkably good activity, despite the presence of substantial steric bulk due to Sn–Bu ligands. The quantitative structure–activity relationship (QSAR) studies for the cytotoxicity of organotin(IV) benzoates, along with some reference drug molecules, is also discussed against a panel of human tumor cell lines. Molecular structures of the tributyltin(IV) complexes (1–4) were fully optimized using the PM6 semi-empirical method and docking studies performed with key enzymes associated with the propagation of cancer, namely ribonucleotide reductase, thymidylate synthase, thymidylate phosphorylase and topoisomerase II. The theoretical results are discussed in relation to the mechanistic role of the cytotoxic active test compounds (1–4).

© 2010 Elsevier Inc. All rights reserved.

1. Introduction

Cisplatin [1–4] was the first inorganic cancer chemotherapeutic agent, and remains a front-line treatment for testicular, ovarian and other cancers. The clinical effectiveness of cisplatin is limited by considerable side effects and the emergence of drug resistance. Consequently new platinum complexes such as carboplatin and oxaliplatin have been approved for clinical use [5].

These advances have spurred a surge of investigations to identify new inorganic agents for use in chemotherapy with improved specificity and decreased toxic side effects. As a result, a great deal of interest in other platinum and non-platinum metalodrugs (e.g., Sn, Ti, Au, Cu, Ru,

and Pd) has emerged that might exhibit comparable cytotoxic properties accompanied by a different pattern of antitumor specificities and by a more favorable pharmacological and toxicological profile [6]. In addition, non-platinum metal-based antitumor agents have been developed where the activity does not rely on direct DNA damage and may involve proteins and enzymes. Metal-based compounds exhibit a wide range of coordination numbers and geometries, significantly increasing the possible spatial arrangements of the ligands and hence the possibility of creating molecules with superior modalities of attack to specific biological targets. Moreover, the redox potential of the metal can interact with the balanced cellular redox state, modifying cell viability either directly or through conversion of a rather inert compound to an activated one, thus tuning the inherent toxicity of the drug.

Among the non-platinum metal compounds with antitumor activity, particular interest has focused on gold and tin derivatives,

* Corresponding author. Tel.: +91 364 2722626; fax: +91 364 2721000.

E-mail addresses: basubaul@nehu.ac.in, basubaul@hotmail.com (T.S. Basu Baul).

which have a common activity on mitochondria and a strong affinity to thiol groups of proteins and enzymes [7–9]. As a result, a large number of organotin(IV) derivatives have been prepared and tested *in vitro* and *in vivo*, firstly against murine leukemia cell lines and then against different panels of human cancer cell lines [10–12]. Several diorganotin(IV) and triorganotin(IV) compounds showed high antiproliferative activity *in vitro* against a variety of solid and hematologic cancers [12,13]. Diorganotin(IV) and triorganotin(IV) terebates and lithoclates, tested against a panel of seven human cancer cell lines, were found to be highly active and more potent than cisplatin. In general, tributyltin(IV) derivatives demonstrated higher efficacy than triphenyltin(IV) and dibutyltin(IV) derivatives [14]. The tributyltin(IV)-3,4-diaminobenzoate, 3,5-diaminobenzoate and 2-[4-(dimethylamino)phenylazo]benzoate were also found to be promising cytostatic agents *in vitro* when tested against human cell line A549 (lung adenocarcinoma) [15]. The cytotoxicity of a tributyltin(IV) lupinylsulfide hydrogen fumarate has also been studied and proved to be extremely active when tested *in vitro* against a panel of tumor cell lines (MCF7, MDA-MB-231 (breast), A2780, OVCAR-3 (ovary), DBTRG-0.5MG, U87 MG, U373 MG, A-172 (glioma) and a mouse glioma cell line (GL261)) and *in vivo* against P388 (myelomonocytic leukemia) and the B16–F10 (melanoma) cell lines [16].

We recently investigated the cytotoxic potential of triphenyltin(IV) 2-[(*E*)-2-(aryl)-1-diazenyl]benzoates and dibutylbis[2-[(*E*)-2-(aryl)-1-diazenyl]benzoato]tin(IV) and found to exhibit high activity when tested *in vitro* against human tumor cell lines [17,18]. Among these, the triphenyltin(IV) compounds were found to be better performers than dibutyltin(IV) compounds. Further, the molecular docking studies of these compounds indicated that the azo group nitrogen atoms and formyl, carbonyl, ester and hydroxyl oxygen atoms in the ligand moiety exhibit hydrogen bonding interactions with the active site of the amino acids of various enzymes, such as ribonucleotide reductase, thymidylate synthase and thymidylate

phosphorylase [17,18]. The high activity was attributed to the presence of an azo group in the organotin(IV) complexes molecules [17,18]. In this paper, we present the synthesis of a new series of complexes where the 2/4-[(*E*)-2-(aryl)-1-diazenyl]benzoate ligands are substituted with tributyltin(IV) (Scheme 1) in the expectation that they will improve dissolution properties and thereby influence cytotoxicity. The tributyltin(IV) complexes, $\text{Bu}_3\text{SnL}^{1-4}\text{H}$ (1–4) were characterized by spectroscopic techniques and crystal structure determination of tributyltin(IV) complex 4. The molecular docking of 1–4 has been investigated with some selected enzymes and preliminary *in vitro* cytotoxicity data are reported for a panel of human tumor cell lines consisting of A498 (renal cancer), EVSA-T (mammary cancer), H226 (non-small-cell lung cancer), IGROV (ovarian cancer), M19 MEL (melanoma), MCF-7 (mammary cancer) and WIDR (colon cancer).

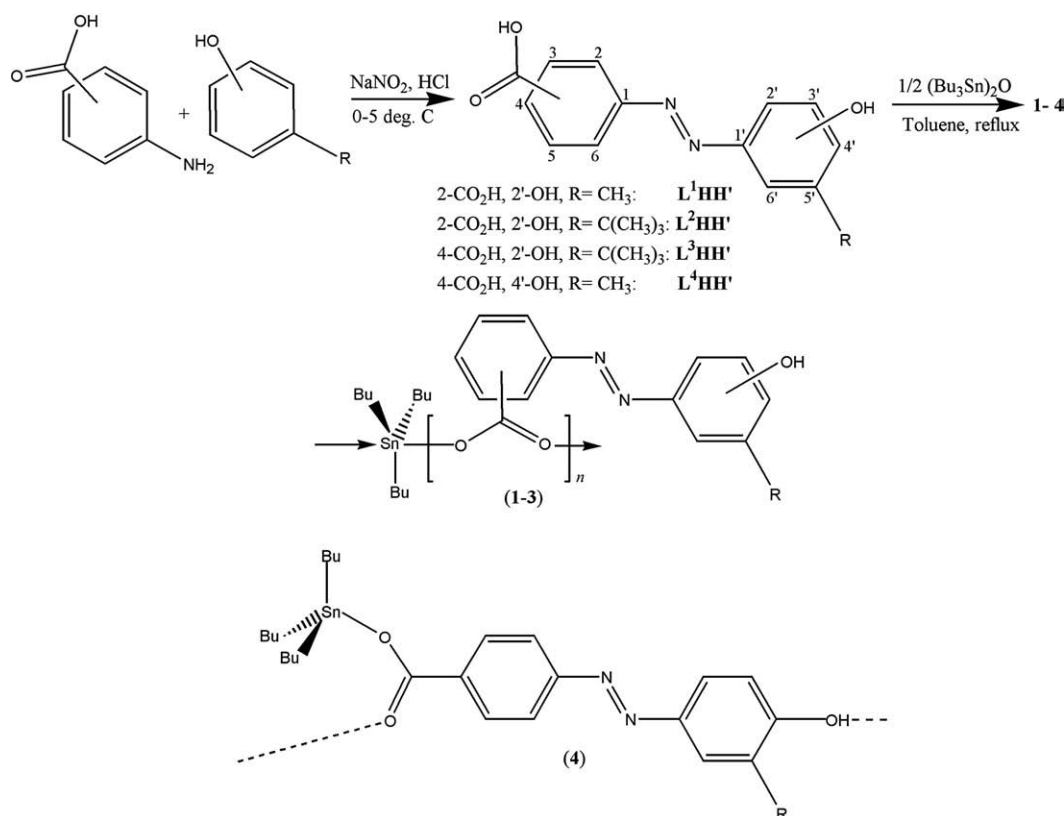
2. Experimental

2.1. Materials and methods

$(\text{Bu}_3\text{Sn})_2\text{O}$, 2-methylphenol, 4-methylphenol, 4-*tert*-butylphenol (Merck), anthranilic acid (Spectrochem), and *p*-aminobenzoic acid (Hi Media) were used without further purification. The solvents used in the reactions were of AR grade and were dried using standard procedures. Toluene was distilled from sodium benzophenone ketyl.

2.2. Synthesis and characterization of ligands

Ligands 2-[(*E*)-(2-hydroxy-5-methylphenyl)diazenyl]benzoic acid ($\text{L}^1\text{HH}'$) [19], 2-[(*E*)-(5-*tert*-butyl-2-hydroxyphenyl)diazenyl]benzoic acid ($\text{L}^2\text{HH}'$) [20], 4-[(*E*)-(5-*tert*-butyl-2-hydroxyphenyl)diazenyl]benzoic acid ($\text{L}^3\text{HH}'$) [18] and 4-[(*E*)-(4-hydroxy-3-methylphenyl)diazenyl]benzoic acid ($\text{L}^4\text{HH}'$) [18] were prepared by the method described in



Scheme 1. Syntheses of ligands $\text{L}^1\text{HH}'$ – $\text{L}^4\text{HH}'$, numbering protocol and the structures of tributyltin(IV) complexes $\text{Bu}_3\text{SnL}^{1-4}\text{H}$ (1–4).

our earlier reports and purities were established from melting point, elemental analysis and ^1H NMR spectroscopy. Abbreviations used for the reported ^1H NMR spectra are as follows: s = singlet, d = doublet, t = triplet, dd = doublet of doublets, dt = doublet of triplets, m = multiplet.

2.3. Synthesis and characterization of tributyltin(IV) complexes

2.3.1. Synthesis of $\text{Bu}_3\text{SnL}^1\text{H}$ (1)

Compound **1** was prepared following the literature method of reacting equimolar amounts of sodium 2-[(*E*)-(2-hydroxy-5-methylphenyl)diazenyl]benzoate and Bu_3SnCl in methanol. The microanalytical and NMR (^1H and ^{13}C , in CDCl_3) data for the complex are in agreement with previous results [19]. The data for ^{117}Sn NMR (CDCl_3): 123.0 ppm and ^{119}Sn Mössbauer, mm s^{-1} : $\delta = 1.50$, $\Delta = 3.85$ [19] are presented here for convenience of the discussion.

2.3.2. Synthesis of $\text{Bu}_3\text{SnL}^2\text{H}$ (2)

Compound **2** was synthesized by mixing $\text{L}^2\text{HH}'$ (0.40 g, 1.34 mmol) and $(\text{Bu}_3\text{Sn})_2\text{O}$ (0.40 g, 0.67 mmol) in 40 ml of anhydrous toluene, in a 100 ml flask equipped with a Dean–Stark moisture trap and a water cooled condenser. The reaction mixture was refluxed for 7 h and the solvent was then removed by distillation. A thick viscous mass was dissolved in small amount of anhydrous benzene, concentrated slowly on a hot plate, cooled to room temperature and petroleum ether added. The pasty mass obtained was triturated in ice-cold conditions which afforded yellow-orange crystalline material. Yield: (0.35 g, 44%). M.p.: 46–48 °C. Anal. calc. for $\text{C}_{29}\text{H}_{44}\text{N}_2\text{O}_3\text{Sn}$: C, 59.30; H, 7.55; N, 4.77 %. Found. C, 58.30; H, 7.80; N, 5.08%. IR (cm^{-1}) 1578 $\nu(\text{OCO})_{\text{asym}}$. ^1H NMR (CDCl_3): δH : Ligand skeleton: 12.6 [brs, 1H, OH], 7.96 [d, 8 Hz, 1H, H3], 7.82 [m, 2H, H6/H6'], 7.47 [t, 8 Hz, 1H, H5], 7.38 [t, 8 Hz, 1H, H4], 7.27 [dd, 2.5, 8 Hz, 1H, H4'], 6.83 [d, 8 Hz, 1H, H3'], 1.30 [s, 9H, CH₃]; Sn–Bu skeleton: 1.61 [m, 6H, H1*], 1.30 [m, 12H, H2* and H3*], 0.82 [t, 9H, H4*] ppm. ^{13}C NMR (CDCl_3): δC : Ligand skeleton: 170.3 [CO₂], 149.5 [C2'], 148.2 [C1], 140.7 [C1'], 136.6 [C4'], 130.8 [C6'], 130.6 [C5], 129.7 [C3], 128.9 [C4], 128.8 [C5'], 128.7 [C2], 117.1 [C3'], 114.7 [C6], 32.9 [C-7'], 30.4 [CH₃]; Sn–Bu skeleton ($^J(^{13}\text{C}-^{119}\text{Sn}, \text{Hz})$): 13.9 [C4*(nd)], 15.7 [C1*(363)], 26.0 [C3*(70)], 26.8 [C2*(20)] ppm. ^{119}Sn NMR (CDCl_3): 124.9 ppm. ^{119}Sn Mössbauer, mm s^{-1} : $\delta = 1.51$, $\Delta = 3.86$, $\Gamma_{\text{av}} = 0.94$; $\rho = 2.44$.

2.3.3. Synthesis of $\text{Bu}_3\text{SnL}^3\text{H}$ (3)

Compound **3** was prepared analogously by following the method and conditions described for **2** and using $\text{L}^3\text{HH}'$ and $(\text{Bu}_3\text{Sn})_2\text{O}$. The pasty mass was dissolved in a benzene–hexane mixture and upon cooling in a refrigerator furnished orange crystalline material of **3**. Yield: 25%. M.p.: 40–42 °C. Anal. calc. for $\text{C}_{29}\text{H}_{44}\text{N}_2\text{O}_3\text{Sn}$: C, 59.30; H, 7.55; N, 4.77 %. Found. C, 58.42; H, 7.70; N, 5.01%. IR (cm^{-1}) 1570 $\nu(\text{OCO})_{\text{asym}}$. ^1H NMR (CDCl_3): δH : ligand skeleton: δH : 12.6 [brs, 1H, OH], 8.16 [dd, 2.5 Hz, 8.0 Hz, 2H, H2/6], 7.89 [m, 3H, H3/5 and H6'], 7.37 [dd, 2.5, 8 Hz, 1H, H4'], 6.92 [d, 8 Hz, 1H, H3'], 1.38 [s, 9H, CH₃]; Sn–Bu skeleton: 1.69 [m, 6H, H1*], 1.38 [m, 12H, H2* and H3*], 0.95 [t, 9H, H4*] ppm. ^{13}C NMR (CDCl_3): δC : Ligand skeleton: 167 [CO₂], 34.0 [C-7'], 31.4 [CH₃], other carbons: 152.8, 150.8, 142.3, 137.1, 133.8, 131.4, 131.2, 129.9, 121.7, 117.9; Sn–Bu skeleton ($^J(^{13}\text{C}-^{119}\text{Sn}, \text{Hz})$): 13.6 [C4*(nd)], 16.6 [C1*(353)], 27.0 [C3*(70)], 27.9 [C2*(20)] ppm. ^{119}Sn NMR (CDCl_3): 120.0 ppm. ^{119}Sn Mössbauer, mm s^{-1} : $\delta = 1.36$, $\Delta = 3.60$, $\Gamma_{\text{av}} = 1.00$; $\rho = 2.65$.

2.3.4. Synthesis of $\text{Bu}_3\text{SnL}^4\text{H}$ (4)

Compound **4** was prepared analogously by following the method and conditions described for **2** and using $\text{L}^4\text{HH}'$ and $(\text{Bu}_3\text{Sn})_2\text{O}$. A thick viscous mass was obtained that was then dissolved in a small amount of hexane and kept in a refrigerator for two weeks. The crystalline material obtained was extracted in hot hexane and filtered. The filtrate upon slow evaporation at room temperature yielded orange

crystals of the desired product. Yield: 28%. M.p.: 80–82 °C. Anal. calc. for $\text{C}_{26}\text{H}_{38}\text{N}_2\text{O}_3\text{Sn}$: C, 57.27; H, 7.02; N, 5.14%. Found. C, 57.40; H, 6.99; N, 5.25%. IR (cm^{-1}) 1606 $\nu(\text{OCO})_{\text{asym}}$. ^1H NMR (CDCl_3): δH : ligand skeleton: OH not detected, 8.18 [dd, 2.5 Hz, 8.0 Hz, 2H, H2/6], 7.87 [dd, 2.5 Hz, 8.0 Hz, 2H, H3/5], 7.79 [d, 2.5 Hz, 1H, H6'], 7.71 [dd, 2.5, 8 Hz, 1H, H2'], 6.91 [d, 8 Hz, 1H, H5'], 2.34 [s, 3H, CH₃]; Sn–Bu skeleton: 1.68 [m, 6H, H1*], 1.38 [m, 12H, H2* and H3*], 0.92 [t, 9H, H4*] ppm. ^{13}C NMR (CDCl_3): δC : ligand skeleton: δC : 171.9 [CO₂], 16.4 [CH₃], other carbons: 158.4, 155.5, 147.2, 133.5, 131.5, 125.8, 125.5, 124.1, 122.5, 115.6; Sn–Bu skeleton ($^J(^{13}\text{C}-^{119}\text{Sn}, \text{Hz})$): 14.1 [C4*(nd)], 17.1 [C1*(363)], 27.4 [C3*(70)], 28.2 [C2*(20)] ppm. ^{119}Sn NMR (CDCl_3): 121.7 ppm. ^{119}Sn Mössbauer, mm s^{-1} : $\delta = 1.39$, $\Delta = 3.04$, $\Gamma_{\text{av}} = 0.87$; $\rho = 2.18$.

2.4. Physical measurements

Carbon, hydrogen and nitrogen analyses were performed with a Perkin Elmer 2400 series II instrument. IR spectra in the range 4000–400 cm^{-1} were obtained on a Perkin Elmer Spectrum BX series FT-IR spectrophotometer with samples investigated as KBr discs. The ^1H and ^{13}C spectra were recorded on a Bruker AMX 400 spectrometer and measured at 400.13 and 100.62 MHz, respectively, while ^{119}Sn NMR spectra were recorded either on a Bruker AMX 400 or a Jeol GX 270 spectrometer and measured at 149.18 and 100.75 MHz, respectively. The ^1H , ^{13}C and ^{119}Sn chemical shifts were referenced to Me_4Si , CDCl_3 and Me_4Sn set at 0.00, 77.0 and 0.00 ppm respectively. The Mössbauer spectra were recorded with a conventional spectrometer operating in the transmission mode. The source was $\text{Ca}^{119}\text{SnO}_3$ (Ritverc GmbH, St. Petersburg, Russia; 10 mCi), moving at room temperature with constant acceleration in a triangular waveform. The driving system, multi-channel analyser, proportional counter gas detector and the related electronics were purchased from Takes (Ponteranica, Bergamo, Italy). The solid absorber samples, containing about 0.5 mg cm^{-2} of ^{119}Sn , were held between aluminum foil windows at 77.3 K in a NRD-1258-DMB liquid–nitrogen cryostat (Cryo Industries, USA). The velocity was calibrated using a 10 mCi ^{57}Co Mössbauer source and 4 μm thick $\alpha^{57}\text{Fe}$ foil as the absorber (both Ritverc GmbH, St. Petersburg, Russia). The isomer shifts are relative to room temperature $\text{Ca}^{119}\text{SnO}_3$.

2.5. Experimental protocol and cytotoxicity tests

The *in vitro* cytotoxicity test of tributyltin(IV) compounds **1–4** was performed using the SRB test for the estimation of cell viability. The human cancer cell lines examined in the present study were WIDR, M19 MEL, A498, IGROV and H226, belonging to the currently used anticancer screening panel of the NCI, USA [21]. The MCF7 cell line is estrogen receptor (ER) +/progesterone receptor (Pgr) + and the cell line EVSA-T is (ER)–/(Pgr)–. Prior to the experiments, a mycoplasma test was carried out on all cell lines and found to be negative. All cell lines were maintained in a continuous logarithmic culture in RPMI 1640 medium with Hepes and phenol red. The medium was supplemented with 10% FCS, 100 $\mu\text{g/ml}$ penicillin and 100 $\mu\text{g/ml}$ streptomycin. The cells were mildly trypsinized for passage and for use in the experiments. RPMI and FCS were obtained from Gibco (Invitrogen, Paisley, Scotland). SRB, DMSO, penicillin and streptomycin were obtained from Sigma (St. Louis MO, USA), TCA and acetic acid from Baker BV (Deventer, NL) and PBS from NPBI BV (Emmer-Compascuum, NL).

The test compounds **1–4** and reference compounds were dissolved at a concentration of 5 mg/ml in DMSO. The compounds were subsequently diluted to a final concentration of 250,000 ng/ml in full medium. Cytotoxicity was estimated by the microculture sulforhodamine B (SRB) test [22].

The experiment was started on day 0. On day 0, 150 μl of trypsinized tumor cells (1500–2000 cells/well) were plated in 96-

wells flat-bottomed micro-titer plates (Cellstar, Greiner Bio-one). The plates were pre-incubated for 48 h at 37 °C, 5% CO₂ to allow the cells to adhere to the bottom. On day 2, a three-fold dilution sequence of ten steps was made in full medium, starting with the 250,000 ng/ml stock solution. Every dilution was used in quadruplicate by adding 50 µl to a column of four wells. This procedure results in the highest concentration of 625,000 ng/ml being present in column 12. Column 2 was used for the blank. Medium was added to column 1 to diminish interfering evaporation.

On day 7, the incubation was terminated. Subsequently, the cells were fixed with 10% trichloroacetic acid in PBS and stored at 4 °C for an hour. After three washings with tap water, the cells were stained for at least 15 min with 0.4% SRB dissolved in 1% acetic acid. After staining, the cells were washed with 1% acetic acid to remove the unbound stain. The plates were air-dried and the bound stain was dissolved in 150 µl 10 mM tris-base. The absorbance was measured at 540 nm using an automated microplate reader (Labsystems Multiskan MS). The data were used for construction of concentration–response curves and determination of the ID₅₀ values using Deltasoft 3 software.

The variability of the *in vitro* cytotoxicity test depends on the cell lines used and the serum applied. With the same batch of cell lines and the same batch of serum the inter-experimental coefficient of variation (CV) is 1–11% depending on the cell line and the intra-experimental CV is 2–4%. These values may be higher with other batches of cell lines and/or serum.

2.6. Quantitative structure–activity relationship (QSAR) methods

The C-QSAR program [23] was used to derive all QSAR models by using multiregression analyses (MRA). In this program, the selection of descriptors has been made on the basis of permutation and correlation matrices among the descriptors in order to avoid collinearity problems. Details of the C-QSAR program, the search engine, the choice of parameters, and their use in the development of QSAR models, have been discussed in previous publications [24,25]. The *in vitro* cytotoxicity data (ID₅₀; ng/ml) of test compounds **1–4** along with some related organotin(IV) azo-compounds (**5–9**) and some standard drug molecules against the seven human tumor cell lines are listed in Table 2. It is preferred in the QSAR analysis that the more effective compounds should have a higher 'activity' and not a lower. Thus, it is very common to transform the concentration of a desired effect 'C' to an activity (negative logarithm of the concentration) by the following equation: $A = -\log C = \log 1/C$, where C is in molar concentration. This is the reason, the cytotoxicity data (Table 2) was first converted into molar concentration (C1–C7), where C1–C7 represent the ID₅₀ (M) values of the organotin(IV) compounds **1–9** along with five anticancer drugs (doxorubicin: DOX, cisplatin: CDDP, 5-fluorouracil: 5-FU, methotrexate: MTX and etoposide: ETO) against the seven human tumor cell lines (A498, EVSA-T, H226, IGROV, M19MEL, MCF-7 and WIDR). Biological parameters for the development of QSAR models are defined by their subsequent dependent variables i.e. activities ($\log 1/C_1$, $\log 1/C_2$, $\log 1/C_3$, $\log 1/C_4$, $\log 1/C_5$, $\log 1/C_6$, and $\log 1/C_7$) (see Tables 3 and 4). $\log P$ is the calculated partition coefficient of a compound in *n*-octanol/water and a measure of its hydrophobicity. HBD is the number of hydrogen bond donors. The value of $\log P$ and HBD were calculated using the ACD PhysChem Suite [26].

In QSAR models, n is the number of data points, r^2 is the square of the correlation coefficient and represents the goodness of fit, q^2 is the cross-validated r^2 , s is the standard deviation, Q is the quality factor, and F is the Fischer ratio. The cross-validated r^2 (q^2) is obtained by using the leave-one-out (LOO) procedure [27]. In each QSAR equation, the value of F in parenthesis refers to their literature value at 95% level [28]. Compound was deemed to be an outlier on the basis of the deviation between observed and predicted activities from the respective QSAR model ($\text{obsd-pred} > 2s$, where s is the standard

deviation) [29]. Each QSAR model includes 95% confidence limits for each term in parentheses. Statistical diagnostics and internal validation (cross-validation and Y -randomization) tests have validated all the QSAR models. The external validation test was not performed due to the small data sets.

2.7. X-ray crystallography

Single crystals of Bu₃SnL⁴H (**4**) suitable for an X-ray crystal structure determination were obtained by slow evaporation of a hexane solution. Crystal data for **4**: C₂₆H₃₈N₂O₃Sn, $M = 545.27$, monoclinic, $P2_1/n$, $a = 9.7101(8)$, $b = 18.6054(16)$, $c = 14.8477(13)$ Å, $\beta = 102.630(2)^\circ$, $V = 2617.5(4)$ Å³, $Z = 4$, $D_x = 1.384$, $F(000) = 1128$, $\mu = 1.004$ mm⁻¹. An orange platelet (0.25 × 0.13 × 0.04 mm) was mounted on a cryo loop and placed directly in the cold stream (130 K) of dinitrogen from an Oxford Cryosystems Cryostream 700 cooler. Intensity data were collected with a Bruker Smart APEX CCD (Mo- K_α radiation, $\lambda = 0.71073$ Å, graphite monochromator) area detector on a D8 goniometer in the ω scan mode. A total of 33,405 reflections were collected within $\theta_{\text{max}} = 27.3^\circ$ and a multi-scan absorption correction [30] was applied. Merging of symmetry equivalent reflections ($R_{\text{int}} = 0.064$) resulted in 5866 unique data, 4351 of these with $I > 2\sigma(I)$. The structure was solved by a Patterson synthesis [31] and refined on F^2 [31]. Carbon atoms C24–C26 associated with one of the *n*-butyl groups were disordered, so two alternative orientations of this moiety were populated in the ratio 0.716(8):0.284(8) and refined with geometry restraints. Isotropic displacement parameters were assigned to the carbon atoms in this disordered part of the structure and anisotropic displacement parameters to all other non-hydrogen atoms. Hydrogen atoms were treated as riding in idealized positions. Convergence was reached for $R = 0.0569$, $wR2 = 0.0844$ and $GOF = 1.050$ for all 5866 data and 292 variables. The residual electron density in a Fourier difference synthesis amounted to 1.2 e·Å⁻³ in the disordered *n*-butyl group. A displacement ellipsoid plot at 50% probability of a molecule in the crystal of **4** is shown in Fig. 2 [30].

2.8. Computational methods

The molecular structures and geometries of the tributyltin(IV) compounds (**1–4**) were fully optimized using the PM6 semiempirical quantum chemistry method [32–36] using the Program CP2K 2.1.7 (Development Version) working with quickstep method [37]. Dockings of compounds (**1–4**) in the active sites of various enzymes are performed using ArgusLab 4.0.1. [32,38–40]. This program was also applied for visualization and molecular modeling of the compounds. The three dimensional coordinates of key enzymes, such as ribonucleotide reductase (pdb ID: 4R1R), thymidylate synthase (pdb ID: 2G8D), thymidylate phosphorylase (pdb ID: 1BRW) and topoisomerase II (pdb ID: 1QZR) were obtained from the Internet at the Research Collaboratory for Structural Bioinformatics (RCSB) Protein Data Bank. The docking program implements an efficient grid-based docking algorithm that approximates an exhaustive search within the free volume of the binding site cavity. The conformational space was explored by the geometry optimization of the flexible ligand (rings are treated as rigid) in combination with the incremental construction of the ligand torsions. Thus, docking occurs between the flexible ligands part of the compounds and enzymes. The ligand orientation is determined by a shape scoring function based on Ascore and the final positions are ranked by lowest interaction energy values. Prior to docking, the ground state was optimized using the PM6QM implemented in the geometry optimization module of program package to confirm that there was no significant divergence in the complex conformations due to crystal packing effects.

3. Results and discussion

3.1. Synthesis and spectroscopy

Ligands L¹HH'–L⁴HH' were prepared by reacting the appropriate *ortho/para*-carboxybenzenediazonium chloride with 2-methylphenol, 4-methylphenol or 4-*tert*-butylphenol in alkaline solution under cold conditions [18–20]. Reaction of L¹HH'–L⁴HH' with (Bu₃Sn)₂O at a 2:1 molar ratio in anhydrous toluene gave tributyltin(IV) complexes Bu₃SnL¹H (1), Bu₃SnL²H (2), Bu₃SnL³H (3) and Bu₃SnL⁴H (4), respectively (Scheme 1).

In solution (CDCl₃), complexes 1–4 exhibited a single sharp ¹¹⁹Sn NMR chemical shift in the range 120–125 ppm that is indicative of a four-coordinate environment at the Sn atom [19,41–43]. The ¹³C NMR spectra displayed the expected carbon signals due to ligand and Sn–Bu skeletons. Assignment of the tri-*n*-butyl ¹³C resonances was based on the ^ηJ(¹³C–^{119/117}Sn) coupling constants. It is known that ^ηJ(¹³C–^{119/117}Sn) coupling constants decrease in the order ¹J(¹³C–^{119/117}Sn) >> ²J(¹³C–^{119/117}Sn) > ³J(¹³C–^{119/117}Sn), depending on ligand properties, and increase with increasing of coordination number at the tin atom [44,45]. The ¹J(¹³C–^{119/117}Sn) coupling constants for complexes 1–4 in CDCl₃ solution are in the range 336–362 Hz, confirming that in solution these compounds have a tetrahedral Sn atom. The ¹H NMR integration values were completely consistent with the formulation of the products. Furthermore, the signals between 12 and 13 ppm observed for CO₂H of the ligands [18–20] were found to be absent in complexes 1–4, confirming the bonding of the carboxylate group to the Sn atom.

The crystal structure of Bu₃SnL¹H (1) has been reported previously and is thus available for comparison [19]. In 1, the carboxylate O atoms of a single aryl ligand bridge two Sn atoms and the pattern then repeats itself to give a continuous single-stranded polymeric structure, as illustrated in Scheme 1. The Sn atoms have a slightly distorted *trans*-R₃SnO₂ trigonal bipyramidal coordination geometry with equatorial butyl groups and two axial carboxylate O atoms, one being from each of two aryl ligands. In contrast, the molecular structure of Bu₃SnL⁴H (4) is best described as four-coordinate with a distorted C₃O tetrahedral geometry involving one of the carboxylate O atoms and three C atoms from the butyl ligands. The molecular structure of 4 is shown in Fig. 1, with selected geometric parameters collected in Table 1. Similar tetrahedral geometry about the Sn atom was observed in (Ph₃Sn[O₂CC₆H₄(N=NC₆H₃-2-OH-5-Me)-o]) and its acetone solvated complex [46,47], (Ph₃Sn{O₂CC₆H₃-*p*-OH[N=N(C₆H₄-X)]} (X = H, 2-Me, 3-Me, 4-Me, 4-OMe, 4-Cl) [41,48,49] and (R₃Sn[O₂CC₆H₄(N=N(C₆H₃-4-OH(C(H)=NC₆H₄X-4)))-o]) (R = Bu

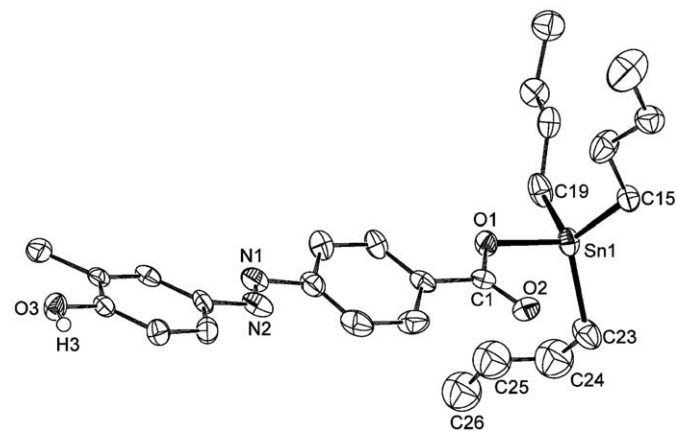


Fig. 1. Displacement ellipsoid plot [30] (50% probability) of a molecule in Bu₃SnL⁴H (4) showing the numbering scheme. H3 has been drawn with arbitrary radius, other hydrogen atoms and the minority conformer of the disordered *n*-butyl group C23–C26 have been omitted.

Table 1

Selected bond lengths (Å) and angles (°)^a obtained from energy minimized structures of the tributyltin(IV) complexes 1–4 and from X-ray crystallography of tributyltin(IV) complex 4.

Bond lengths (Å) and angles (°)	1	2	3	4	
					X-ray
Sn(1)–O(1)	2.161	2.166	2.149	2.142	2.083(2)
Sn(1)–O(2)	2.952	2.939	3.028	3.064	2.982(2)
Sn(1)–C(15)	2.150	2.150	2.151	2.151	2.129(3)
Sn(1)–C(19)	2.154	2.154	2.154	2.155	2.129(3)
Sn(1)–C(23)	2.149	2.149	2.150	2.149	2.143(4)
O(1)–C(1)	1.321	1.321	1.321	1.322	1.295(4)
O(2)–C(1)	1.234	1.235	1.228	1.227	1.222(4)
N(1)–N(2)	1.260	1.260	1.260	1.256	1.225(4)
O(1)–Sn(1)–O(2)	47.7	47.8	46.8	46.2	47.8(7)
O(1)–Sn(1)–C(15)	102.1	102.1	101.8	101.6	104.3(11)
O(1)–Sn(1)–C(19)	95.2	94.8	94.2	95.9	97.5(12)
O(1)–Sn(1)–C(23)	103.3	103.2	104.9	103.7	105.2(12)
O(2)–Sn(1)–C(15)	84.0	82.7	86.7	86.1	84.3(11)
O(2)–Sn(1)–C(19)	142.3	142.3	139.7	140.9	144.4(11)
O(2)–Sn(1)–C(23)	73.9	74.8	73.3	73.1	76.8(11)
C(15)–Sn(1)–C(19)	115.3	115.5	116.1	115.7	117.2(14)
C(19)–Sn(1)–C(23)	117.1	117.3	117.1	117.1	112.0(15)
C(15)–Sn(1)–C(23)	118.3	118.1	117.4	117.6	117.3(14)
Sn(1)–O(1)–C(1)	115.4	114.9	116.9	118.0	115.6(2)
Sn(1)–O(2)–C(1)	79.2	79.6	76.4	75.4	73.8(17)
O(1)–C(1)–O(2)	117.7	117.6	119.9	120.3	122.8(3)

^a For energy minimized structures of compounds 1 and 4, refer to Figs. 4 and 5 and for compounds 2 and 3, refer to Figs. S1 and S2. Refer to Fig. 1 for atom numbering schemes.

and Ph; X = Me and Br) [42]. The other carboxylate O atom of the benzoate ligand also coordinates weakly to the Sn atom with the Sn(1)–O(2) distance being 2.982(2) Å. This interaction is the cause of the distortion of the tetrahedral primary coordination sphere, but the Sn(1)–O(2) distance is considered to be too long for the Sn atom to be described as truly five-coordinate. In addition, the bond angles around the Sn atom in 4 are more consistent with a tetrahedral environment than with a trigonal bipyramidal five-coordinate environment. Compound 4 exhibits the usual distorted tetrahedral structural motif in which the phenoxy hydrogen atom of the carboxylate ligand forms an intermolecular hydrogen bond with the non-coordinating carbonyl O atom of the carboxylate group of a neighbouring molecule; the O···O donor–acceptor distance in this interaction amounts to 2.778(3) Å. Fig. 2 (see Scheme 1 for schematic representation) illustrates how this translation results in infinite chains extending along [010].

Mössbauer spectroscopy was used to obtain insight into the solid-state structures of complexes 2 and 3, for which no suitable crystals could be obtained for X-ray crystallography. Typically, one doublet spectra with narrow average full width at half maximum of the resonant peaks (Γ_{av} , 0.87–1.00 mm s^{−1}), characteristic of occurrence of unique tin coordination site, were obtained for all four compounds. From the deconvolution of the obtained spectra, isomer shifts (δ) of 1.51 (2), 1.36 (3), and 1.39 (4) mm s^{−1}, typical of organotin(IV) derivatives [50], were extracted and a similar value ($\delta = 1.51$ mm s^{−1}) was observed earlier for 1 [19].

The tributyltin(IV) complexes 2 and 3 exhibited very similar ¹¹⁹Sn Mössbauer spectra characterized by $|\Delta_{exp}|$ values of 3.86 and 3.60 mm s^{−1}, respectively, which are characteristic of trigonal bipyramidal structures with butyl groups in equatorial position and axial electronegative ligands. A similar value ($\Delta = 3.85$ mm s^{−1}) was found earlier for the complex 1 which was characterized crystallographically [19] and displayed a distorted *trans*-R₃SnO₂ trigonal bipyramidal coordination geometry in the polymer. The $|\Delta_{exp}|$ values for the complexes 1–3 are in the same order of magnitude, suggesting that they assume the same structural motif as depicted in Scheme 1. The crystallographic data presented above for complex 4 show that the carboxylate moiety acts as a monodentate ligand, giving rise to a distorted C₃O tetrahedral geometry involving one of the carboxylate O atoms and the C atoms from the three butyl ligands. On this basis, a

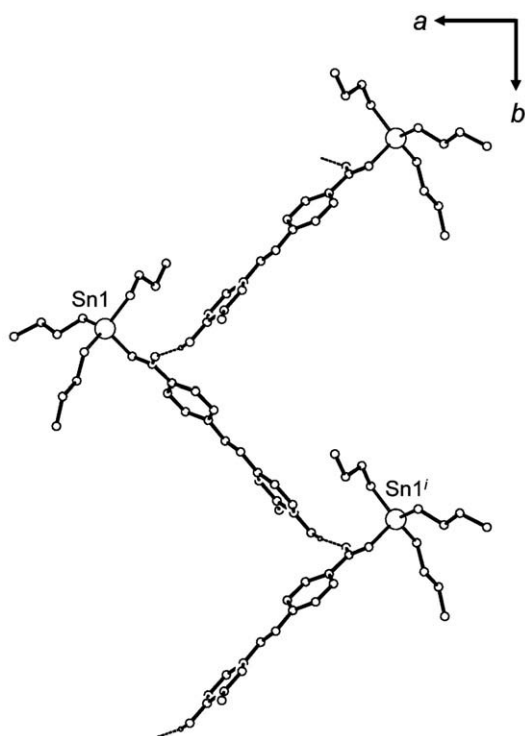


Fig. 2. A segment of the chain formed by hydrogen bonds in $\text{Bu}_3\text{SnL}^4\text{H}$ (**4**). The view direction is slightly inclined to $[001]$ for clarity. Symmetry operator $i = -1/2 - x, 1/2 + y, 1/2 - z$.

point charge model formalism [51] has been applied for complex **4**, using $\{\text{Bu}\}^{\text{tet}} = -1.13 \text{ mm s}^{-1}$ [52], $\{\text{COO}^-\}^{\text{tet bridging}} = 0.1145 \text{ mm s}^{-1}$ calculated from $[\text{COO}^-]^{\text{tba}}$ [53] (tet = tetrahedral, tba = trigonal bipyramidal axial), considering a tetrahedral structure of the complex where three positions are occupied by the butyl groups and the fourth by an oxygen donor of a bridging carboxylate (see Fig. 3) and the Δ_{calcd} value was found to be -2.97 mm s^{-1} .

The $|\Delta_{\text{exp}}|$ value of 3.04 mm s^{-1} observed for complex **4** corresponds well with that of the Δ_{calcd} value and is within the range of 2.3 – 3.0 mm s^{-1} , characteristic for four-coordinate tetrahedral geometry [50]. Further, the $|\Delta_{\text{exp}}|$ value is comparable with that of $(\text{Bu}_3\text{Sn}[\text{O}_2\text{C}_6\text{H}_4\{\text{N}=\text{N}(\text{C}_6\text{H}_3-4\text{-OH}(\text{C}(\text{H})=\text{NC}_6\text{H}_4\text{Br}-4)\})-p])$, which has also been characterized crystallographically [42]. The ratio of the quadrupole splitting to isomer shift value ($\rho = |\Delta_{\text{exp}}|/\delta$) can be used to distinguish between the different coordination states of the central tin atom [50]. Tributyltin(IV) complexes **1**, **2** and **3** have ρ values in the range 2.44 – 2.65 , suggestive of a five-coordinated tin geometry, while complex **4** has a ρ value of 2.18 , indicative of a four-coordinated tin environment, as reflected in the crystal structure, and in agreement with reported ρ values for similar tetrahedral tributyltin(IV) complexes [35]. Using the Parish relationship between the $|\Delta_{\text{exp}}|$

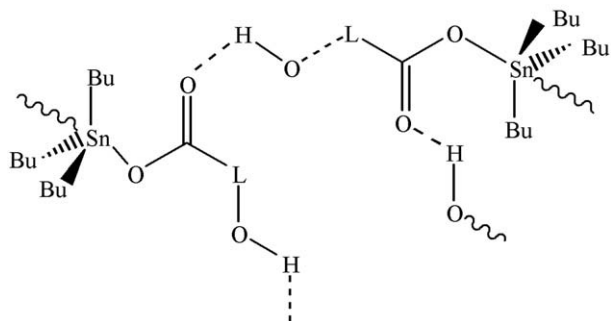


Fig. 3. A line diagram showing chain structure of $\text{Bu}_3\text{SnL}^4\text{H}$ (**4**).

value and C–Sn–O bond angle [51], the calculated C–Sn–O angle in **4** was found to be 109° , in reasonable conformity with that derived from X-ray crystallography.

The solid-state IR spectra of the complexes display a strong, sharp band due to the $[\nu_{\text{asym}}(\text{OCO})]$ stretching vibration at $\sim 1575 \text{ cm}^{-1}$ for **1** and **2** and $\sim 1605 \text{ cm}^{-1}$ for **3** and **4** as a result of carboxylate coordination to the Sn atom [41,42,48,49]. This compares to bands at $\sim 1700 \text{ cm}^{-1}$ ($\text{L}^{1-2}\text{HH}'$) [20] and $\sim 1685 \text{ cm}^{-1}$ ($\text{L}^{3-4}\text{HH}'$) [18] for the free ligands. The assignment of the symmetric $[\nu_{\text{sym}}(\text{OCO})]$ stretching vibration band could not be made owing to the complex pattern of the spectra.

3.2. Quantum chemical calculations

The geometries of the tributyltin(IV) complexes **1–4** were fully optimized using the semi-empirical method (PM6). Harmonic frequency calculations were performed for all the stationary points to characterize their nature and to ensure that the optimized structures correspond to global minima. The molecular structures of **1** and **4** obtained after full geometry optimization at PM6 levels are shown in Figs. 4 and 5 (for the structures of **2** and **3** refer to S1 and S2), respectively, while the optimized geometric parameters are collected in Table 1. The X-ray experimental geometrical parameters for **4** are also included in Table 1, which match closely with that of calculated values for **4**. Most of the geometric parameters for **1–4** are found to be insensitive to the nature of the substituents R (see Scheme 1). Since the basic structures and coordination geometry of tributyltin(IV) complexes **1–4** are similar despite the differently substituted ligands, it may be expected that the ligand properties have a direct influence on the stability of the corresponding tributyltin(IV) complexes, as well as on their cytotoxic activity (see below).

3.3. Cytotoxicity studies

The *in vitro* cytotoxic results for organotin(IV) compounds of formulations $\text{Bu}_3\text{SnL}^{1-4}\text{H}$ (**1–4**), $\text{Ph}_3\text{SnL}^{5-6}\text{H}$ (**5–6**) [17] and $\text{Bu}_2\text{Sn}(\text{L}^{1-3}\text{H})_2$ (**7–9**) [18] were investigated across the panel of human tumor cell lines A498, EVSA-T, H226, IGROV, M19 MEL, MCF-7 and WIDR, as per NCI protocol (Table 2). The cytotoxicity data (ID_{50}) for the test compounds (**1–4**) are of the same order of magnitude and the change of ligand substitution does not improve the cytotoxic activity significantly. Upon closer inspection of the ID_{50} values of **1–4**, one can see that $\text{Bu}_3\text{SnL}^1\text{H}$ (**1**) was more cytotoxic than the other test compounds (**2–4**). A marginal decrease in activity was seen on increasing the steric bulk further at the coupling site of the ligand framework by the addition of a *tert*-butyl group, as in compound **2**. The change of tributyltin ester from *ortho*- (**2**) to *para*-position (**3**) did not yield any change in cytotoxic activity except for the EVSA-T (mammary cancer) cell line, which showed substantial increase in activity ($\text{ID}_{50} = 27 \text{ ng/ml}$). Changing substituents i.e. tributyltin ester and hydroxyl group from *ortho*- (**1**) to *para*-position (**4**) have demonstrated lesser activity. Thus, it can be inferred that the substituents in the ligand skeleton play a vital role in determining the cytotoxic potentials of a compound. In general, the cytotoxic results of compounds **1–4** are undoubtedly far superior to CDDP, 5-FU and ETO and related dibutyltin(IV) compounds **7–9**. While test compounds **1–4** in this investigation displayed comparable activity to triphenyltin(IV) compounds **5** and **6** [17] across a panel of seven human tumor cell lines, compounds **1–4** have the advantage of higher solubility. The activity has been attributed to the tetrahedral geometry of the complexes in solution, as well as the presence of an azo functionality in the ligand framework, and was subsequently confirmed by docking results [17,18]. Ruthenium complexes containing azo-ligands have also shown higher activity in comparison to the complexes with non-azo-ligands [54,55]. Promising cytotoxic activity was also noted for the related tributyltin(IV) 2-[4-(dimethylamino)phenylazo]benzoate, $\text{Bu}_3\text{Sn}[\text{O}_2\text{C}_6\text{H}_4(\text{N}=\text{NC}_6\text{H}_4\text{N}(\text{CH}_3)_2-4)-\text{O}]$,

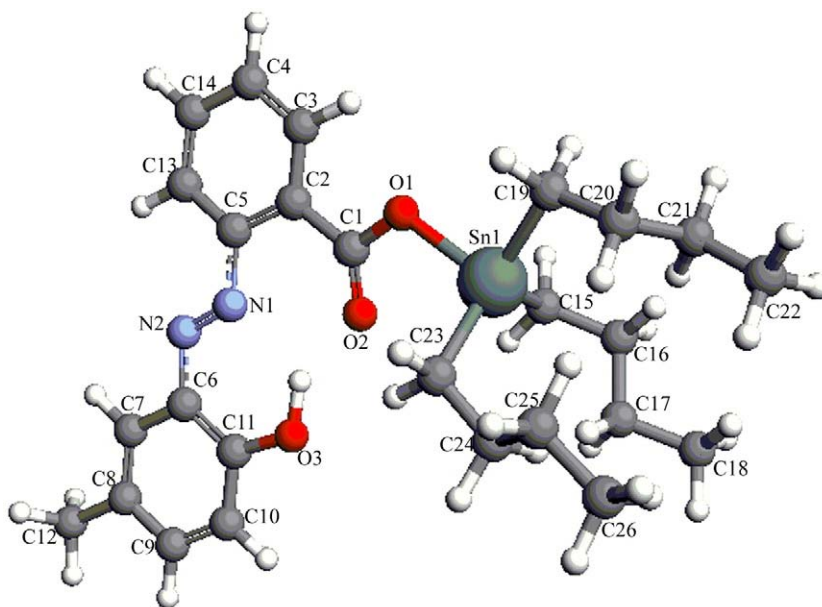


Fig. 4. The structure of $\text{Bu}_3\text{SnL}^{\text{H}}$ (**1**) obtained after full geometry optimization.

which also contains an azo group, when tested *in vitro* against Human cell line A549 (lung adenocarcinoma) [15]. Thus, the cytotoxicity data of compound **1**, together with its better solubility, suggest it might be a promising candidate for further *in vitro* and *in vivo* studies after appropriate modifications. The cytotoxicity data of compounds **1–4** indicate that structural variation of the Sn–R and L–R skeletons influence the activity. However, the reason behind factors influencing the activity of these compounds is yet to be fully understood and more *in vitro* and *in vivo* studies are needed in order to derive structure–activity relationships for these kinds of complexes.

3.4. QSAR Studies

From the data in Table 3, the following QSAR models 1–7 were developed:

QSAR for the cytotoxicity of compounds **1–9** against A498 cancer cell line (Table 3)

$$\log 1/C1 = -0.17(\pm 0.06)\log P + 7.65(\pm 0.46) \quad (1)$$

$$n = 8, r^2 = 0.876, s = 0.113, q^2 = 0.797, Q = 8.283,$$

$$F_{1,6} = 42.387(5.987)$$

Outlier: compound **7**

QSAR for the cytotoxicity of compounds **1–9** against EVSA-T cancer cell line (Table 3)

$$\log 1/C2 = -0.13(\pm 0.09)\log P + 7.71(\pm 0.66) \quad (2)$$

$$n = 7, r^2 = 0.729, s = 0.155, q^2 = 0.557, Q = 5.510,$$

$$F_{1,5} = 13.450(6.608)$$

Outlier: compounds **3** and **7**

QSAR for the cytotoxicity of compounds **1–9** against H226 cancer cell line (Table 3)

$$\log 1/C3 = -0.16(\pm 0.05)\log P + 7.63(\pm 0.41) \quad (3)$$

$$n = 9, r^2 = 0.882, s = 0.120, q^2 = 0.831, Q = 7.825,$$

$$F_{1,7} = 52.322(5.591)$$

QSAR for the cytotoxicity of compounds **1–9** against IGROV cancer cell line (Table 3)

$$\log 1/C4 = -0.18(\pm 0.07)\log P + 7.65(\pm 0.52) \quad (4)$$

$$n = 8, r^2 = 0.864, s = 0.129, q^2 = 0.787, Q = 7.209,$$

$$F_{1,6} = 38.118(5.987)$$

Outlier: compound **7**

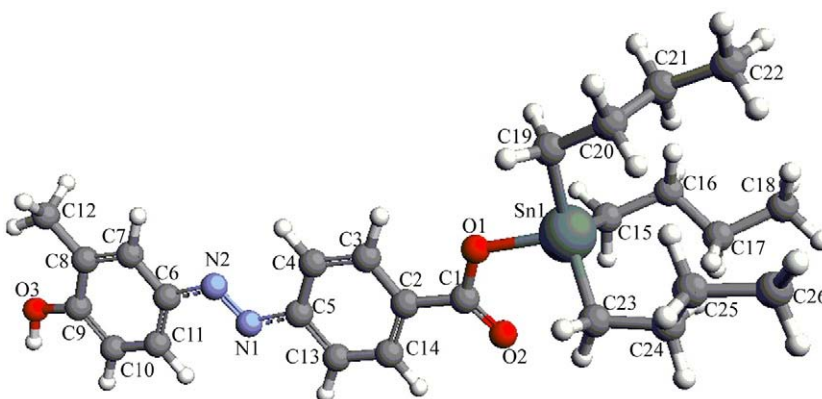


Fig. 5. The structure of $\text{Bu}_3\text{SnL}^{\text{H}}$ (**4**) obtained after full geometry optimization.

Table 2*In vitro* ID₅₀ values (ng/ml) of test compounds **1–4**, related organotin(IV) azo-compounds **5–9** and some standard drugs against seven human tumor cell lines.^a

Test compound ^b	Cell lines						
	A498	EVSA-T	H226	IGROV	M19 MEL	MCF-7	WIDR
Bu ₃ SnL ⁵ H (1)	162	97	148	214	118	113	106
Bu ₃ SnL ² H (2)	176	100	165	253	126	120	105
Bu ₃ SnL ³ H (3)	177	27	167	269	127	112	105
Bu ₃ SnL ⁴ H (4)	182	101	163	239	125	118	106
Ph ₃ SnL ⁵ H (5) ^c [17]	101	41	104	109	103	92	104
Ph ₃ SnL ⁶ H (6) ^c [17]	103	49	101	101	104	78	95
Bu ₂ Sn(L ² H) ₂ (7) ^c [18]	429	134	816	617	374	236	896
Bu ₂ Sn(L ³ H) ₂ (8) ^c [18]	1169	371	1140	1489	901	416	2125
Bu ₂ Sn(L ⁴ H) ₂ (9) ^c [18]	382	134	497	449	294	162	551
DOX	90	8	199	60	16	10	11
CDDP	1503	493	645	229	711	653	576
5-FU	143	475	340	297	442	750	225
MTX	37	5	2287	7	23	18	<3.2
ETO	1314	317	3934	580	505	2594	150
TAX	<3.2	<3.2	<3.2	<3.2	<3.2	<3.2	<3.2

^a Abbreviation: DOX, doxorubicin; CDDP, cisplatin; 5-FU, 5-fluorouracil; MTX, methotrexate; ETO, etoposide and TAX, paclitaxel.^b Standard drug reference values are cited immediately after the test compounds under identical conditions. For compounds **5** and **6**, the reference values for CDDP were 2253, 422, 3269, 169, 558, 699 and 967 for A498, EVSA-T, H226, IGROV, M19 MEL, MCF-7 and WIDR cell lines, respectively.^c Reported triphenyltin(IV) and dibutyltin(IV) compounds (**5–9**) have been included for comparison; see refs. 17,18: LH is a carboxylate residue where L⁵H, 2-[(E)-2-(4-hydroxy-5-methylphenyl)-1-diazenyl]benzoate and L⁶H, 2-[(E)-2-(3-formyl-4-hydroxyphenyl)-1-diazenyl]benzoate while all other LH are described in Scheme 1.QSAR for the cytotoxicity of compounds **1–9** against M19 MEL cancer cell line (Table 3)

$$\log 1/C5 = -0.15(\pm 0.06) \log P + 7.64(\pm 0.42) \quad (5)$$

$$n = 8, r^2 = 0.874, s = 0.104, q^2 = 0.664, Q = 8.990,$$

$$F_{1,6} = 41.619(5.987)$$

Outlier: compound **7**QSAR for the cytotoxicity of compounds **1–9** against MCF-7 cancer cell line (Table 3)

$$\log 1/C6 = -0.10(\pm 0.05) \log P + 7.36(\pm 0.32) \quad (6)$$

$$n = 8, r^2 = 0.823, s = 0.080, q^2 = 0.587, Q = 11.338,$$

$$F_{1,6} = 27.898(5.987)$$

Outlier: compound **7****Table 3**Biological and hydrophobicity (log *P*) parameters of compounds **1–9** used to derive QSARs 1–7.

No.	Compound	log1/C1 (Eq. (1))			log1/C2 (Eq. (2))			log1/C3 (Eq. (3))		
		Obsd.	Pred.	Δ	Obsd.	Pred.	Δ	Obsd.	Pred.	Δ
1	1	6.53	6.65	-0.12	6.75	6.93	-0.18	6.57	6.65	-0.08
2	2	6.52	6.42	0.10	6.77	6.76	0.01	6.55	6.43	0.12
3 ^b	3	6.52	6.40	0.12	7.34	6.74	0.60	6.55	6.41	0.14
4	4	6.48	6.63	-0.15	6.73	6.92	-0.19	6.52	6.63	-0.11
5	5	6.78	6.70	0.08	7.17	6.97	0.20	6.76	6.70	0.06
6	6	6.78	6.72	0.06	7.10	6.99	0.11	6.79	6.73	0.06
7 ^{a,b}	7	6.29	5.92	0.37	6.79	6.37	0.42	6.01	5.95	0.06
8	8	5.85	5.88	-0.03	6.35	6.34	0.01	5.86	5.91	-0.05
9	9	6.29	6.35	-0.06	6.74	6.71	0.03	6.17	6.37	-0.20
No.	Compound	log1/C1 (Eq. (4))			log1/C2 (Eq. (5))			log1/C3 (Eq. (6))		
		Obsd.	Pred.	Δ	Obsd.	Pred.	Δ	Obsd.	Pred.	Δ
1	1	6.41	6.56	-0.15	6.66	6.73	-0.07	6.68	6.78	-0.10
2	2	6.37	6.32	0.05	6.67	6.52	0.15	6.69	6.65	0.04
3	3	6.34	6.30	0.04	6.67	6.51	0.16	6.72	6.64	0.08
4	4	6.36	6.54	-0.18	6.64	6.71	-0.07	6.66	6.77	-0.11
5	5	6.74	6.62	0.12	6.77	6.78	-0.01	6.82	6.81	0.01
6	6	6.79	6.64	0.15	6.77	6.80	-0.03	6.90	6.82	0.08
7 ^a	7	6.13	5.78	0.35	6.34	6.07	0.27	6.54	6.36	0.18
8	8	5.74	5.73	0.01	5.96	6.03	-0.07	6.30	6.34	-0.04
9	9	6.22	6.25	-0.03	6.40	6.46	-0.06	6.66	6.61	0.05
No.	Compound	log1/C7 (Eq. (7))			log <i>P</i>					
		Obsd.	Pred.	Δ	Obsd.	Pred.	Δ			
1	1	6.71	6.77	-0.06	5.94	5.94	0.00			
2	2	6.75	6.48	0.27	7.27	7.27	0.00			
3	3	6.75	6.46	0.29	7.38	7.38	0.00			
4	4	6.71	6.75	-0.04	6.05	6.05	0.00			
5	5	6.76	6.84	-0.08	5.63	5.63	0.00			
6	6	6.81	6.87	-0.06	5.49	5.49	0.00			
7	7	5.97	5.84	0.13	10.23	10.23	0.00			
8	8	5.59	5.79	-0.20	10.46	10.46	0.00			
9	9	6.13	6.40	-0.27	7.66	7.66	0.00			

^a Not included in the derivation of QSAR 1, 4, 5, 6.^b Not included in the derivation of QSAR 2.

QSAR for the cytotoxicity of compounds **1–9** against WIDR cancer cell line (Table 3)

$$\log 1 / C7 = -0.22(\pm 0.09) \log P + 8.06(\pm 0.69) \quad (7)$$

$$n = 9, r^2 = 0.818, s = 0.205, q^2 = 0.700, Q = 4.415,$$

$$F_{1,7} = 31.462(5.591)$$

Molecular hydrophobicity of organotin(IV) compounds **1–9** is found to be the single most important parameter for all the QSAR models 1–7. Based on deviations ($\text{obsd} - \text{pred} > 2 \times s$), compound **7** behaves as a common outlier for five of the seven QSAR models (QSARs 1, 2, 4, 5 and 6). While the exact reason for **7** being an outlier is not clear, comparison with dibutyltin(IV) compounds **8** and **9**, which have the same skew trapezoidal geometry, indicates that steric factors may play a critical role for the unusual activity of **7**. To assess the effects of excluding outliers, QSAR models were examined before and after the removal of compound. The linear $\log P$ models 1–7 with negative coefficients suggest that the cytotoxicity of compounds **1–9** decreases with increasing hydrophobicity against all seven cancer cell lines (A498, EVSA-T, H226, IGROV, M19MEL, MCF-7 and WIDR). Although there are high statistics associated with QSARs 1–7 ($r^2 = 0.729$ – 0.882), the existence of linear correlations between activity and hydrophobicity of the compounds is not great enough to establish the upper limit of the activity. Since $\log P$ of compounds **1–9** are very high (5.49–10.46), these compounds may have more than the optimum $\log P$ value. This suggests that QSARs 1–7 may represent only the second half of the parabolic/bilinear model in terms of $\log P$ and may be the cause of the negative $\log P$ term in all QSARs. Thus, more compounds with lower $\log P$ ($\log P < 5.49$) values will be needed to establish the upper $\log P$ limit either by the development of a parabolic or bilinear QSAR model. To solve this problem, QSAR models 8–14 were developed using the same cytotoxicity data of compounds **1–9** along with that of anticancer drugs DOX, CDDP, 5-FU, MTX, and ETO. These drug molecules have $\log P$ values ranging from -2.53 to 0.28 , which may represent the first half of the parabolic/bilinear model and may then be helpful in establishing the optimum $\log P$ value for the series of compounds (**1–9**).

QSAR for the cytotoxicity of compounds **1–9** along with five anticancer drugs (DOX, CDDP, 5-FU, MTX and ETO) against A498 cancer cell line (Table 4)

$$\log 1 / C1 = 0.23(\pm 0.08) \log P - 0.02(\pm 0.01) \log P^2 + 5.95(\pm 0.22)$$

$$n = 12, r^2 = 0.844, s = 0.201, q^2 = 0.692, Q = 4.572, \quad (8)$$

$$F_{2,9} = 24.346(4.257)$$

Optimum $\log P = 5.41(4.59$ – $6.87)$ Outliers: DOX and MTX

QSAR for the cytotoxicity of compounds **1–9** along with five anticancer drugs (DOX, CDDP, 5-FU, MTX and ETO) against EVSA-T cancer cell line (Table 4)

$$\log 1 / C2 = 0.41(\pm 0.14) \log P - 0.03(\pm 0.02) \log P^2 \quad (9)$$

$$+ 0.37(\pm 0.13) \text{HBD} + 5.28(\pm 0.58)$$

$$n = 14, r^2 = 0.839, s = 0.318, q^2 = 0.658, Q = 2.881,$$

$$F_{3,10} = 17.371(3.708)$$

Optimum $\log P = 5.99(5.06$ – $7.63)$.

QSAR for the cytotoxicity of compounds **1–9** along with five anticancer drugs (DOX, CDDP, 5-FU, MTX, and ETO) against H226 cancer cell line (Table 4)

$$\log 1 / C3 = 0.38(\pm 0.12) \log P - 0.03(\pm 0.01) \log P^2 + 5.50(\pm 0.28)$$

$$n = 12, r^2 = 0.866, s = 0.229, q^2 = 0.745, Q = 4.061, \quad (10)$$

$$F_{2,9} = 29.082(4.257)$$

Optimum $\log P = 5.78(5.11$ – $6.88)$. Outliers: DOX and CDDP

QSAR for the cytotoxicity of compounds **1–9** along with five anticancer drugs (DOX, CDDP, 5-FU, MTX, and ETO) against IGROV cancer cell line (Table 4)

$$\log 1 / C4 = 0.30(\pm 0.13) \log P - 0.03(\pm 0.01) \log P^2$$

$$+ 0.35(\pm 0.14) \text{HBD} + 5.46(\pm 0.54) \quad (11)$$

$$n = 12, r^2 = 0.854, s = 0.251, q^2 = 0.629, Q = 3.681,$$

$$F_{3,8} = 15.598(4.067)$$

Optimum $\log P = 4.75(3.87$ – $5.73)$ Outliers: DOX and ETO

QSAR for the cytotoxicity of compounds **1–9** along with five anticancer drugs (DOX, CDDP, 5-FU, MTX, and ETO) against M19MEL cancer cell line (Table 4)

$$\log 1 / C5 = 0.36(\pm 0.09) \log P - 0.03(\pm 0.01) \log P^2$$

$$+ 0.30(\pm 0.09) \text{HBD} + 5.34(\pm 0.38) \quad (12)$$

$$n = 14, r^2 = 0.898, s = 0.209, q^2 = 0.767, Q = 4.536,$$

$$F_{3,10} = 29.346(3.708)$$

Optimum $\log P = 5.51(4.90$ – $6.34)$

QSAR for the cytotoxicity of compounds **1–9** along with five anticancer drugs (DOX, CDDP, 5-FU, MTX, and ETO) against MCF-7 cancer cell line (Table 4)

$$\log 1 / C6 = 0.39(\pm 0.10) \log P - 0.03(\pm 0.01) \log P^2$$

$$+ 0.35(\pm 0.09) \text{HBD} + 5.20(\pm 0.40) \quad (13)$$

$$n = 13, r^2 = 0.921, s = 0.209, q^2 = 0.746, Q = 4.589,$$

$$F_{3,9} = 34.975(3.863)$$

Optimum $\log P = 5.98(5.27$ – $7.01)$ Outlier: ETO

QSAR for the cytotoxicity of compounds **1–9** along with five anticancer drugs (DOX, CDDP, 5-FU, MTX, and ETO) against WIDR cancer cell line (Table 4)

$$\log 1 / C7 = 0.38(\pm 0.07) \log P - 0.04(\pm 0.01) \log P^2$$

$$+ 0.28(\pm 0.08) \text{HBD} + 5.66(\pm 0.30) \quad (14)$$

$$n = 12, r^2 = 0.955, s = 0.152, q^2 = 0.811, Q = 6.428,$$

$$F_{3,8} = 56.593(4.067)$$

Optimum $\log P = 4.72(4.35$ – $5.12)$ outlier: Compound **9**

All the above QSAR models (8–14) are parabolic correlations in terms of $\log P$, which suggest that the cytotoxic activity of these compounds first increases with an increase in their hydrophobicity up to an optimum $\log P$ and then decreases, as defined by the equations for respective cancer cell lines. The optimum $\log P$ for QSAR models 8–14 range from 4.72 to 5.99. HBD is present in five QSAR models (Eqs. (9), (11)–(14)) and its positive coefficient suggest that the cytotoxic activity of these compounds, against five respective cancer cell lines, increases with increase in the number of hydrogen bond donor. On the other hand, it has been suggested by Lipinski et al. that a $\text{HBD} \leq 5$

Table 4Biological, hydrophobicity (log *P*), and HBD parameters of compounds **1–9** along with five anticancer drugs (DOX, CDDP, 5-FU, MTX, and ETO) used to derive QSARs 8–14.

No.	Compound	log1/C1 (Eq. (8))			log1/C2 (Eq. (9))			log1/C3 (Eq. (10))		
		Obsd.	Pred.	Δ	Obsd.	Pred.	Δ	Obsd.	Pred.	Δ
1	1	6.53	6.57	−0.04	6.75	6.88	−0.13	6.57	6.59	−0.02
2	2	6.52	6.51	0.01	6.77	6.83	−0.06	6.55	6.52	0.03
3	3	6.52	6.50	0.02	7.34	6.82	0.52	6.55	6.51	0.04
4	4	6.48	6.57	−0.09	6.73	6.88	−0.15	6.52	6.59	−0.07
5	5	6.78	6.58	0.20	7.17	6.88	0.29	6.76	6.59	0.17
6	6	6.78	6.58	0.20	7.10	6.87	0.23	6.79	6.59	0.20
7	7	6.29	6.08	0.21	6.79	6.64	0.15	6.01	5.94	0.07
8	8	5.85	6.04	−0.19	6.35	6.57	−0.22	5.86	5.88	−0.02
9	9	6.29	6.47	−0.18	6.74	7.16	−0.42	6.17	6.47	−0.30
10 ^{a,b}	DOX	6.78	6.01	0.77	7.83	8.00	−0.17	6.44	5.59	0.85
11 ^b	CDDP	5.30	5.23	0.07	5.78	5.52	0.26	5.67	4.34	1.33
12	5-FU	5.96	5.79	0.17	5.44	5.75	−0.31	5.58	5.24	0.34
13 ^a	MTX	7.09	5.84	1.25	7.96	7.71	0.25	5.30	5.33	−0.03
14	ETO	5.65	6.02	−0.37	6.27	6.52	−0.25	5.17	5.60	−0.43
No.	Compound	log1/C4 (Eq. (11))			log1/C5 (Eq. (12))			log1/C6 (Eq. (13))		
		Obsd.	Pred.	Δ	Obsd.	Pred.	Δ	Obsd.	Pred.	Δ
1	1	6.41	6.47	−0.06	6.66	6.63	0.03	6.68	6.69	−0.01
2	2	6.37	6.32	0.05	6.67	6.54	0.13	6.69	6.64	0.05
3	3	6.34	6.30	0.04	6.67	6.52	0.15	6.72	6.63	0.09
4	4	6.36	6.47	−0.11	6.64	6.63	0.01	6.66	6.69	−0.03
5	5	6.74	6.49	0.25	6.77	6.64	0.13	6.82	6.69	0.13
6	6	6.79	6.50	0.29	6.77	6.64	0.13	6.90	6.69	0.21
7	7	6.13	5.94	0.19	6.34	6.20	0.14	6.54	6.46	0.08
8	8	5.74	5.86	−0.12	5.96	6.13	−0.17	6.30	6.39	−0.09
9	9	6.22	6.61	−0.39	6.40	6.78	−0.38	6.66	6.95	−0.29
10 ^c	DOX	6.96	8.01	−0.05	7.53	7.50	0.03	7.74	7.71	0.03
11	CDDP	6.12	5.93	0.19	5.63	5.40	0.23	5.66	5.40	0.26
12	5-FU	5.64	5.97	−0.33	5.47	5.69	−0.22	5.24	5.63	−0.39
13	MTX	7.81	7.80	0.01	7.30	7.25	0.05	7.40	7.44	0.04
14 ^{c,d}	ETO	6.01	6.60	−0.59	6.07	6.33	−0.26	5.36	6.34	−0.98
No.	Compd.	log1/C7 (Eq.(14))			log <i>P</i>	HBD				
		Obsd.	Pred.	Δ						
1	1	6.71	6.78	−0.07	5.94	1				
2	2	6.75	6.58	0.17	7.27	1				
3	3	6.75	6.55	0.20	7.38	1				
4	4	6.71	6.77	−0.06	6.05	1				
5	5	6.76	6.81	−0.05	5.63	1				
6	6	6.81	6.82	−0.01	5.49	1				
7	7	5.97	5.90	0.07	10.23	2				
8	8	5.59	5.79	−0.20	10.46	2				
9 ^e	9	6.13	6.77	−0.64	7.66	2				
10	DOX	7.69	7.72	−0.03	0.24	7				
11	CDDP	5.72	5.56	0.16	−2.53	4				
12	5-FU	5.76	5.95	−0.19	−0.65	2				
13	MTX	–	7.45	–	−0.45	7				
14	ETO	6.59	6.60	−0.01	0.28	3				

^a Not included in the derivation of QSAR 8.^b Not included in the derivation of QSAR 10.^c Not included in the derivation of QSAR 11.^d Not included in the derivation of QSAR 13.^e Not included in the derivation of QSAR 14.

improves oral bioavailability [56]. The organotin(IV) compounds of the present investigation **1–9** have HBD values of either 1 or 2. This means that we have room to increase the HBD and improve the activity of these compounds. Although the HBD term is present in five QSARs, log *P* is the most important indicator of compound activity and explains the major part of the variance in the data. Thus most attention should be paid to the hydrophobicity of the compounds.

3.4.1. Validation of QSAR models 1–14

All QSAR models (1–14) were validated in two steps involving statistical diagnostics and internal validation. In statistical diagnostics, QSAR models 1–14 were filtered through the following seven necessary conditions: (i) $n/p \geq 4$ (ii) $r^2 > 0.6$ (iii) $q^2 > 0.5$ (iv) $r^2 - q^2 < 0.3$ (v) $F > F_{(lit)}$ at 95% level (vi) high *Q* value, and (vii) low *s* value [28,57–61]. Internal

validation was carried out using cross-validation ($q^2 > 0.5$) and Y-randomization tests [59,62] (see Table 5). In the Y-randomization tests, the poor values of r^2 and q^2 ensure the robustness of QSAR models 1–14 and also the lack of over fitting. Due to the small data sets, the external validation test was not considered.

3.4.2. Comparative QSAR study on the cytotoxic activities of compounds **1–9** against seven cancer cell lines (A498, EVSA-T, H226, IGROV, M19 MEL, MCF-7 and WIDR)

On comparison among QSAR models 1–7, one can suggest that the mechanism for the cytotoxic activity of compounds **1–9** against A498, EVSA-T, H226, IGROV, M19 MEL, MCF-7 and WIDR cancer cell lines is almost the same and directly dependent on the hydrophobicity of the compound. It must be noted here that QSARs 1 and 3–7

Table 5
Y-Randomization test data for QSARs 1–14.

QSAR No.	NOR-1 ^a		NOR-2		NOR-3		NOR-4		NOR-5	
	r ²	q ²	r ²	q ²	r ²	q ²	r ²	q ²	r ²	q ²
1	0.699	0.047	0.003	-0.679	0.392	-0.210	0.011	-0.763	0.008	-0.374
2	0.567	-0.440	0.081	-0.621	0.397	-0.193	0.048	-0.675	0.021	-0.441
3	0.488	0.083	0.010	-0.544	0.486	0.090	0.120	-0.393	0.037	-0.293
4	0.676	-0.086	0.033	-0.635	0.309	-0.306	0.003	-0.791	0.092	-0.782
5	0.620	-0.025	0.010	-0.636	0.424	-0.226	0.095	-0.614	0.321	-0.377
6	0.501	-0.597	0.002	-0.646	0.324	-0.309	0.002	-0.335	0.089	-0.850
7	0.419	-0.005	0.068	-0.417	0.517	0.111	0.273	-0.142	0.513	0.226
8	0.435	-0.096	0.445	0.189	0.430	-0.028	0.240	-0.391	0.031	-0.781
9	0.415	-0.150	0.341	-0.106	0.466	-0.139	0.564	0.154	0.244	-0.353
10	0.236	-0.070	0.557	0.312	0.121	-0.406	0.376	0.037	0.041	-0.475
11	0.778	-0.491	0.490	-1.268	0.596	-2.079	0.538	-1.395	0.334	-1.960
12	0.393	-0.213	0.390	-0.021	0.404	-0.329	0.552	0.137	0.177	-0.463
13	0.435	-0.251	0.358	-0.153	0.368	-0.810	0.266	-0.988	0.211	-0.411
14	0.466	-1.401	0.250	-2.121	0.423	-2.015	0.525	-1.147	0.714	-0.179

^a NOR = number of Y-randomization.**Table 6**
Correlations among the cytotoxic activities of compounds 1–9 against seven cancer cell lines e.g. A498, EVSA-T, H226, IGROV, M19 MEL, MCF-7, and WIDR.

QSAR no.	QSAR models (n = 9)	r ²	q ²	s
15	log 1/C1 = 0.76 log 1/C2 + 1.23	0.628	0.085	0.185
16	log 1/C1 = 0.82 log 1/C3 + 1.17	0.904	0.768	0.094
17	log 1/C1 = 0.89 log 1/C4 + 0.80	0.968	0.927	0.055
18	log 1/C1 = 1.05 log 1/C5 - 0.39	0.947	0.921	0.070
19	log 1/C1 = 1.62 log 1/C6 - 4.33	0.940	0.914	0.074
20	log 1/C1 = 0.58 log 1/C7 + 2.69	0.844	0.712	0.120
21	log 1/C2 = 0.65 log 1/C3 + 2.70	0.518	0.245	0.220
22	log 1/C2 = 0.70 log 1/C4 + 2.39	0.557	0.383	0.211
23	log 1/C2 = 0.85 log 1/C5 + 1.28	0.581	0.427	0.205
24	log 1/C2 = 1.39 log 1/C6 - 2.42	0.642	0.517	0.189
25	log 1/C2 = 0.46 log 1/C7 + 3.86	0.495	0.204	0.225
26	log 1/C3 = 0.98 log 1/C4 + 0.21	0.875	0.819	0.124
27	log 1/C3 = 1.19 log 1/C5 - 1.37	0.920	0.655	0.099
28	log 1/C3 = 1.76 log 1/C6 - 5.32	0.834	0.713	0.143
29	log 1/C3 = 0.71 log 1/C7 + 1.85	0.935	0.886	0.090
30	log 1/C4 = 1.10 log 1/C5 - 0.86	0.862	0.779	0.124
31	log 1/C4 = 1.79 log 1/C6 - 5.59	0.945	0.900	0.079
32	log 1/C4 = 0.60 log 1/C7 + 2.44	0.747	0.597	0.169
33	log 1/C5 = 1.46 log 1/C6 - 3.19	0.884	0.784	0.096
34	log 1/C5 = 0.58 log 1/C7 + 2.82	0.956	0.883	0.060
35	log 1/C6 = 0.33 log 1/C7 + 4.52	0.766	0.555	0.088

explain 82.3–88.2% of the variance in the data sets either without or with one outlier. On the other hand, QSAR 2 explains only 72.9% of the variance in the data set with two outliers. The poor statistics of QSAR 2 compared to the other QSAR models (Eqs. (1) and (3)–(7)) suggest that it may have an additional mechanism to the common one.

Similar/dissimilar mechanisms involved in the cytotoxic activity of compounds 1–9 against seven different cancer cell lines (A498, EVSA-T, H226, IGROV, M19 MEL, MCF-7 and WIDR) can also be understood by direct comparison among their activities, known as activity–activity relationships. Correlations among the cytotoxic activities of compounds 1–9 against seven different cancer cell lines are given in Table 6 (Eq. (15)–(35)). The high mutual correlations among the cytotoxicities against six cancer cells in QSARs 16–20 ($r^2/q^2 = 0.904/0.768, 0.968/0.927, 0.947/0.921, 0.940/0.914, \text{ and } 0.844/0.712$) suggest that compounds 1–9 may obey a similar mechanism for their cytotoxicities against six cancer cells (A498, H226, IGROV, M19MEL, MCF-7 and WIDR), as shown in Fig. 6. On the other hand, the invalid QSARs 15, 21, 22, 23, and 25 ($r^2/q^2 = 0.628/0.085, 0.518/0.245, 0.557/0.383, 0.581/0.427 \text{ and } 0.495/0.204$) suggest that the mechanism for the cytotoxicities of compounds 1–9 against EVSA-T cancer cell line is different to that of the other five cancer cell lines (A498, H226, IGROV, M19 MEL and WIDR). The poor statistics, but valid QSAR 24 ($r^2/q^2 = 0.642/0.517$), suggest that there is some similarity in the mechanism for the cytotoxicities of compounds 1–9 against EVSA-T

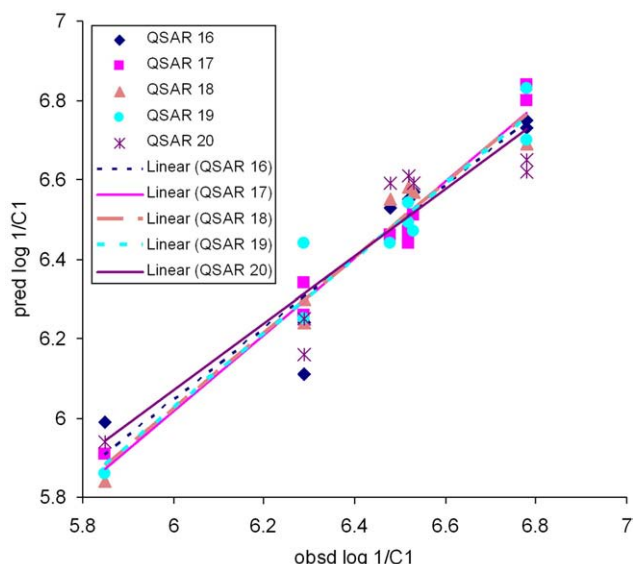


Fig. 6. Plot of observed log 1/C1 versus predicted log 1/C1 from QSARs 16–20 (Table 6).

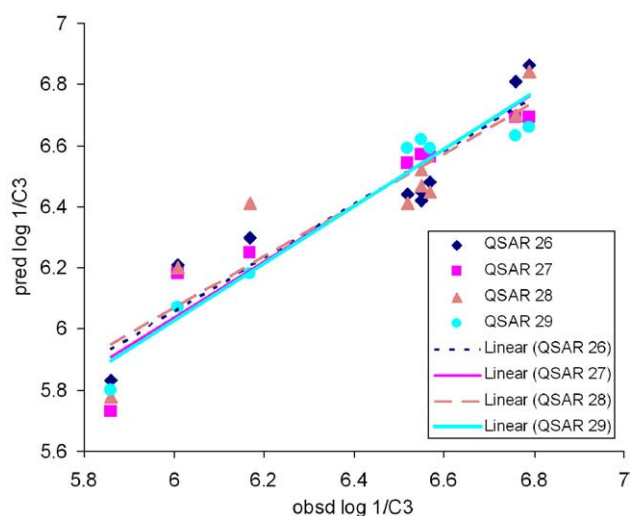


Fig. 7. Plot of observed log 1/C3 versus predicted log 1/C3 from QSARs 26–29 (Table 6).

and MCF-7 cell lines. This is not surprising because both are breast cancer cell lines. EVSA-T and MCF-7 are the ER⁻/PR⁺ and ER⁺/PR⁺ breast cancer cell lines, respectively. Although the similarity between these two breast cancer cell lines is due to the progesterone receptor-positive (PR⁺), the dissimilarity is due to the estrogen receptor-negative/positive (ER⁻/ER⁺). The similar cytotoxic mechanism for compounds **1–9** among the five cancer cell lines H226, IGROV, M19 MEL, MCF-7 and WIDR has been further supported by their high mutual correlations, as shown by QSARs 26–35 (Table 6) and Figs. 7–10. From the above discussions, it can be suggested that the cytotoxicities of compounds **1–9** against six cancer cell lines (A498, H226, IGROV, M19MEL, MCF-7 and WIDR) are due to a similar mechanism, but the same is not true against EVSA-T cancer cell.

3.5. Docking study

Dockings of compounds **1–4** in the active sites of the key enzymes RNR, TS, TP and topoII have been determined since these enzymes are promising targets for cancer therapy. For example, RNR performs a key, rate limiting step in DNA synthesis, controls the balance of the deoxyribonucleotide pools, and changes in its activity can alter the spontaneous mutation rate of cells [63]. Increased RNR activity has been associated with disease states including cancer [63,64] and inhibition of this enzyme is an attractive target for cancer therapy.

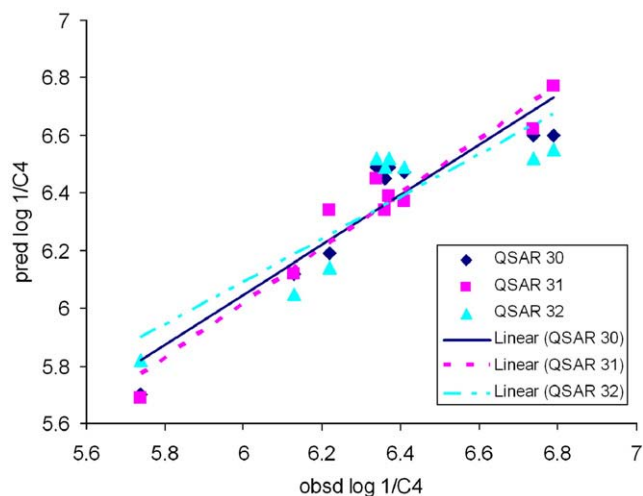


Fig. 8. Plot of observed log 1/C4 versus predicted log 1/C4 from QSARs 30–32 (Table 6).

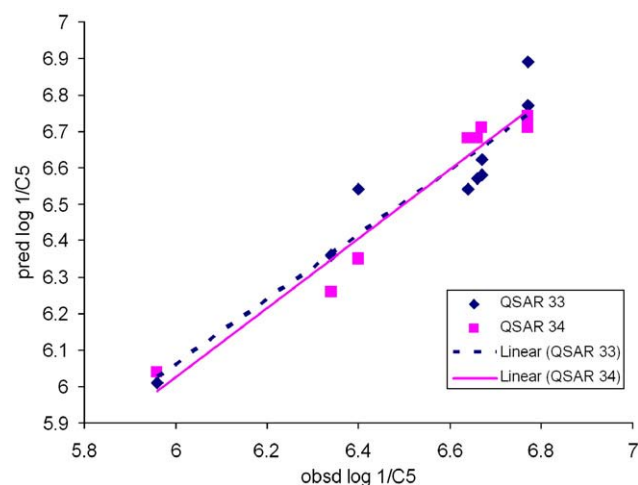


Fig. 9. Plot of observed log 1/C5 versus predicted log 1/C5 from QSARs 33 and 34 (Table 6).

Studies on the effect of iron, copper, and zinc ions on RNR in freshly isolated normal and leukemic human lymphocytes found that zinc acts to inhibit the enzyme in both cell types, while iron and copper had stimulatory effects [63,64]. Metal complexes of carbothioamides [65–67] and thiosemicarbazones [68] have been found to inhibit RNR and possess anticancer activity. On the other hand, anthracyclines and some V(IV) and Mo(IV) compounds have been shown to exert various effects on DNA or inhibit topoII [69,70]. Recently, information has been acquired from the enzymes docking studies of compounds **5** and **6** [17] and **7–9** [18]. Combined with the encouraging cytotoxic activity obtained for test compounds **1–4**, this prompted us to carry out molecular docking studies of **1–4** to understand and hopefully overcome some of the challenges occurring by formation of strong covalent attachments to target enzymes.

The results of docking studies of **1** and **4** with enzymes are shown in Figs. 11–18 while results for **2** and **3** can be seen in S3–S10. The docking program is validated by docking ADP in the active site of enzyme RNR, with a close overlap between the docked ligand and the native ligand being observed [17]. The docking studies revealed that tributyltin(IV) compounds **1–4** interact with enzymes RNR (4R1R), TS (2G8D), TP (1BRW) and topoII (1QZR) at various sites and their hydrogen bonding interactions are given in Table 7. All compounds exhibited hydrogen bonding interactions through azo nitrogen atom (s) with amino acid residues of the enzymes RNR, TS and TP. Both azo group N(1) and N(2) atoms of compounds **1** and **2** interacted with RNR, while there was interaction with either N(1) or N(2) for the

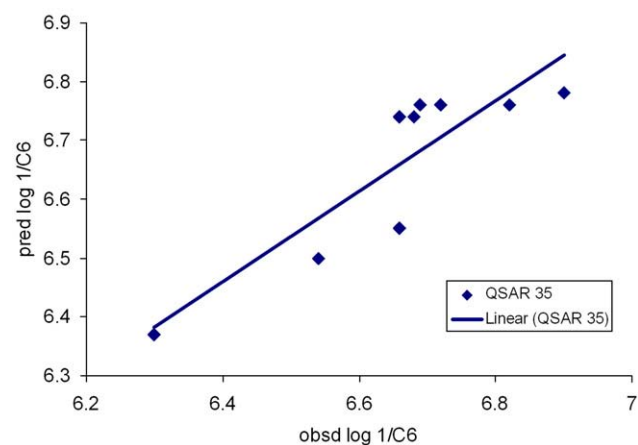


Fig. 10. Plot of observed log 1/C6 versus predicted log 1/C6 from QSAR 35 (Table 6).

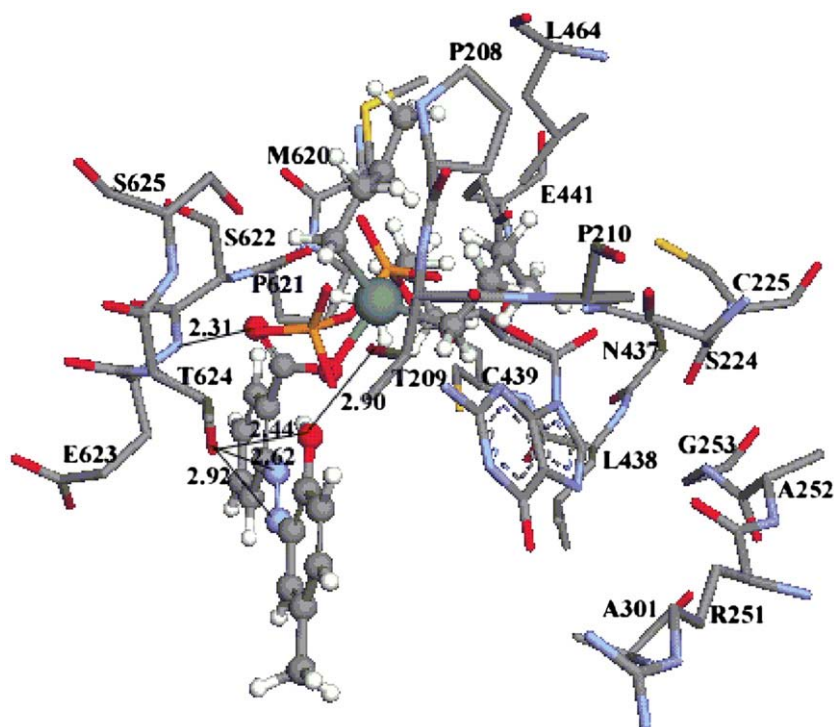


Fig. 11. $\text{Bu}_3\text{SnL}^1\text{H}$ (**1**) docked into the binding site of the enzyme ribonucleotide reductase (4R1R). Hydrogen bonding interactions between the various groups of **1** and amino acid residues are shown. Hydrogen atoms are omitted for clarity.

other enzymes. Hydroxyl group oxygen atom(s) of the compounds show more hydrogen bonding interactions with active sites of the enzymes than other functional groups of the compounds (Table 7, see

Figs. 11–18 and S3–S10 for specific amino acid residues). It should be mentioned that tributyltin(IV) compounds **1**, **2** and **4** exhibited hydrogen bonding interactions through Sn–oxygen atom(s) with

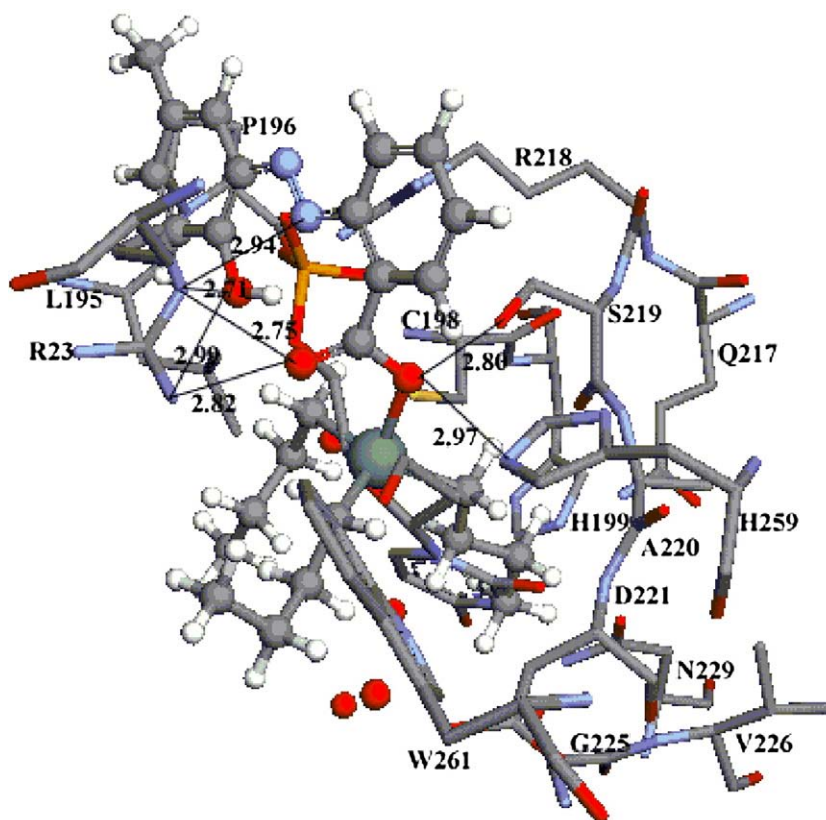


Fig. 12. $\text{Bu}_3\text{SnL}^1\text{H}$ (**1**) docked into the binding site of the enzyme thymidylate synthase (2G8D). Hydrogen bonding interactions between the various groups of **1** and amino acid residues are shown. Hydrogen atoms are omitted for clarity.

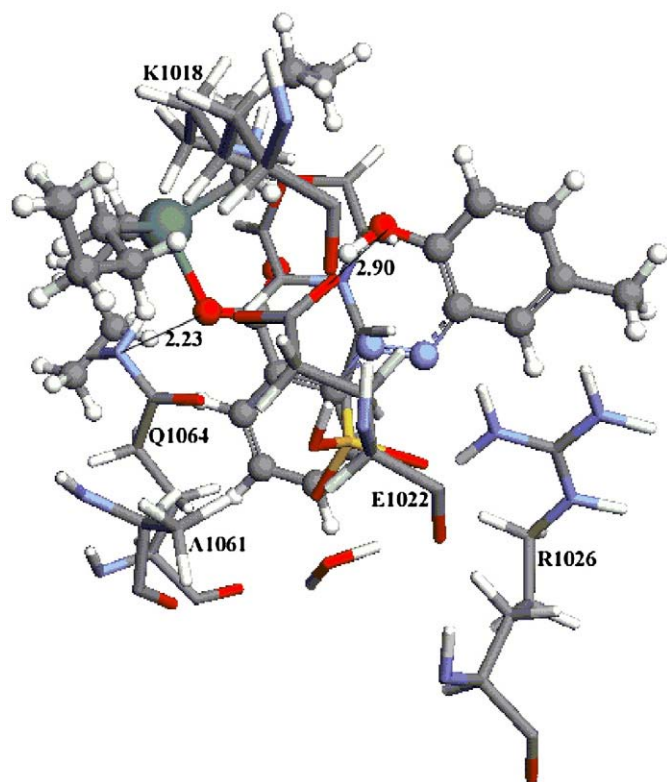


Fig. 13. $\text{Bu}_3\text{SnL}^1\text{H}$ (**1**) docked into the binding site of the enzyme thymidylate phosphorylase (1BRW). Hydrogen bonding interactions between the various groups of **1** and amino acid residues are shown. Hydrogen atoms are omitted for clarity.

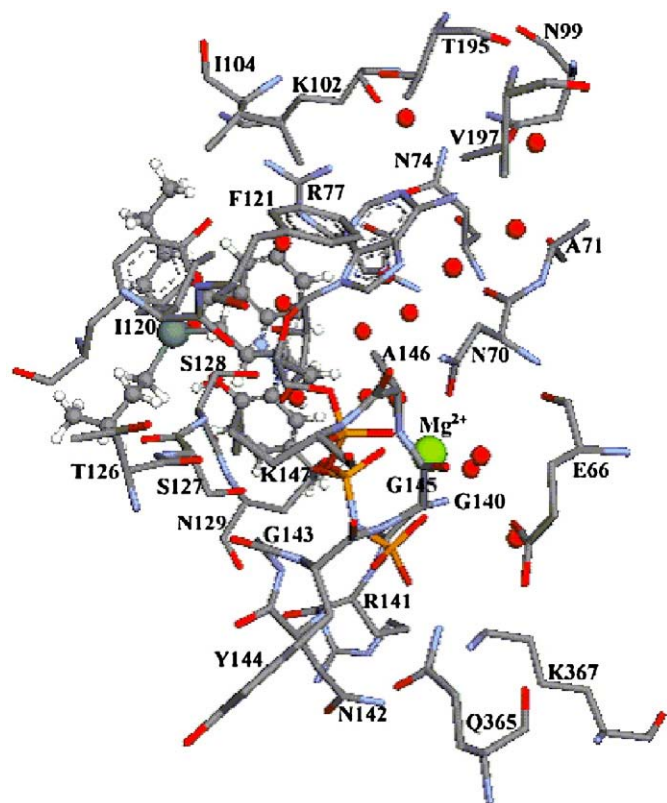


Fig. 14. $\text{Bu}_3\text{SnL}^1\text{H}$ (**1**) docked into the binding site of the enzyme topoisomerase II (1QZR). Hydrogen bonding interactions between the various groups of **1** and amino acid residues are shown. Hydrogen atoms are omitted for clarity.

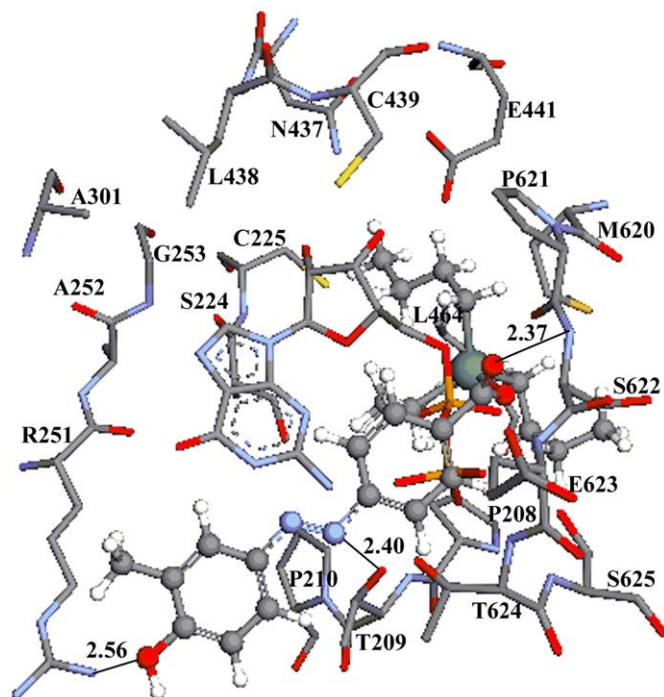


Fig. 15. $\text{Bu}_3\text{SnL}^4\text{H}$ (**4**) docked into the binding site of the enzyme ribonucleotide reductase (4R1R). Hydrogen bonding interactions between the various groups of **4** and amino acid residues are shown. Hydrogen atoms are omitted for clarity.

enzymes TS, TP and topoll and that such interactions were not observed earlier for triphenyltin(IV) compounds (**5** and **6**) [17] and dibutyltin(IV) compounds (**7–9**) [18].

Docking studies also revealed that compounds **1–4** are masked inside the active site of topoll and exhibited hydrogen bonding interactions through various atoms of the molecule with amino acid residues of the enzyme, for instance R77 (in compound **2**), K102 (in compound **3**), S127, G143, T195 and S127 (in compound **4**). Such interactions were not observed at all earlier for compounds **5–9** [17,18].

Therefore, on the basis of docking studies, it is inferred that the anticancer activities of compounds **1–4** might be emanating from their interactions with enzymes RNR, TS, TP and topoll. The docking studies also indicate that the azo group nitrogen atoms, hydroxyl, carbonyl oxygen atoms and Sn–oxygen atom in the ligand moiety play an important role during the dockings of the tributyltin(IV) compounds into the active sites of various enzymes. Nevertheless, the possibility of coordination through tin beyond the active site of the enzymes cannot be ruled out completely. It is very difficult to envisage the role of such atoms in binding proteins in relation to improved cytotoxic activity.

4. Conclusions and outlook

The present series of tributyltin(IV) 2/4-[(*E*)-2-(aryl)-1-diazenyl] benzoates (**1–4**) was designed to provide a new skeletal framework that incorporates a tributyltin(IV) ester and a ligand that varies in both the position of the carboxylate and OH, Me and *tert*-Bu substituents. It was anticipated that this variation would determine the number of possible hydrogen bonds between a complex and enzyme amino acid residues and hence influence the activity of the compounds. In solution, the organotin(IV) benzoates exist as four-coordinate tetrahedral tin species, while in the solid-state they have either a distorted tetrahedral (**4**) or distorted trigonal bipyramidal geometry (**1–3**). Promising cytotoxic effects were noted for the complexes, with $\text{Bu}_3\text{SnL}^1\text{H}$ (**1**) being more cytotoxic than the other test compounds (**2–4**). In general, the cytotoxic results of compounds

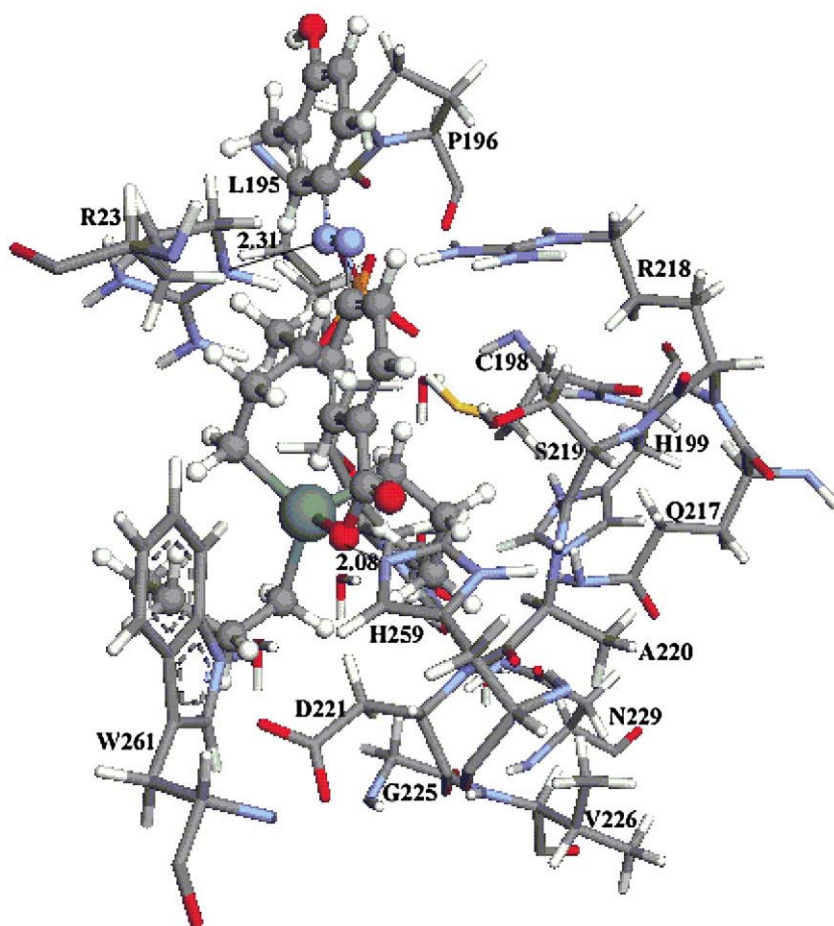


Fig. 16. $\text{Bu}_3\text{SnL}^4\text{H}$ (**4**) docked into the binding site of the enzyme thymidylate synthase (2G8D). Hydrogen bonding interactions between the various groups of **4** and amino acid residues are shown. Hydrogen atoms are omitted for clarity.

1–4 are far superior to CDDP, 5-FU, ETO and related dibutyltin(IV) compounds **7–9**, and comparable to their triphenyltin(IV) analogues **5** and **6** across a panel of seven human tumor cell lines. Docking studies

of compounds **1–4** indicated that the cytotoxic activity may be associated with the tetrahedral geometry of the complexes in solution and the presence of an azo functionality in the ligand framework. The

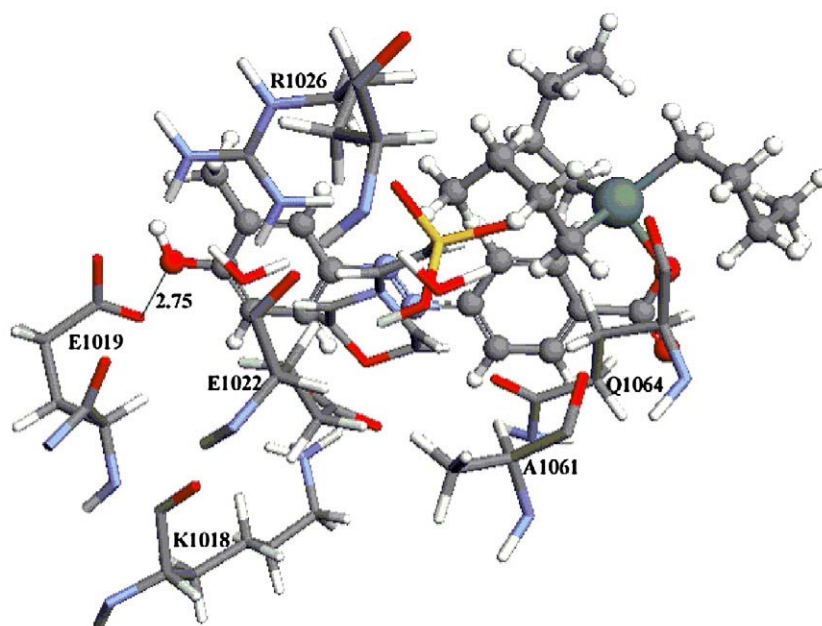


Fig. 17. $\text{Bu}_3\text{SnL}^4\text{H}$ (**4**) docked into the binding site of the enzyme thymidylate phosphorylase (1BRW). Hydrogen bonding interactions between the various groups of **4** and amino acid residues are shown. Hydrogen atoms are omitted for clarity.

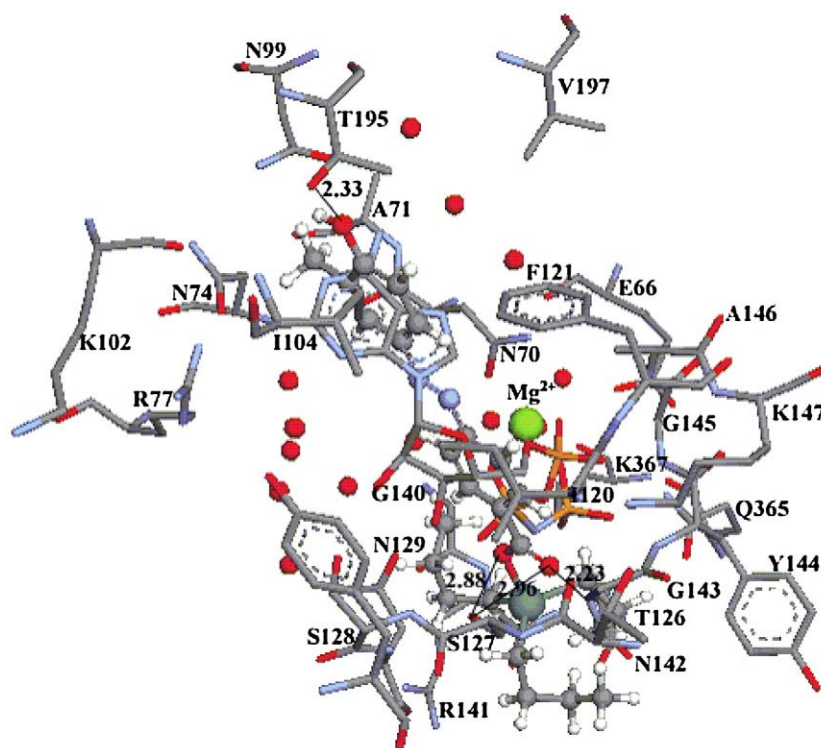


Fig. 18. $\text{Bu}_3\text{SnL}^4\text{H}$ (**4**) docked into the binding site of the enzyme topoisomerase II (1QZR). Hydrogen bonding interactions between the various groups of **4** and amino acid residues are shown. Hydrogen atoms are omitted for clarity.

potential of these tributyltin(IV) complexes as enzyme inhibitors was shown by the exquisite binding and highly specific target enzymes recognition. Careful characterization of kinetics and enzyme/inhibitor complex structures is necessary to truly demonstrate specificity. Thus, the docking studies are very important since disease pathology often correlates with abnormal enzyme activity and therefore enzyme inhibition can be a powerful and versatile tool in the treatment of disease. Data from the present study suggests that the tributyltin(IV) complex **1** merits further investigation as a new drug and may be a suitable candidate for modification in order to improve cytotoxic and dissolution properties. Further work in this area is underway.

Acknowledgements

The financial support of the Department of Science and Technology, New Delhi, India (grant nos. SR/S1/IC-03/2005,TSBB and SR/S1/OC-11A/2006, PS), the Università degli Studi di Palermo, Italy (grants ORPA079E5M and ORPA0737W2, LP) and the University Grants Commission, New Delhi, India through SAP-DSA, Phase-III, are gratefully acknowledged. The *in vitro* cytotoxicity experiments were carried out by Ms. P. F. van Cuijk in the Laboratory of Translational Pharmacology, Department of Medical Oncology, Erasmus Medical Centre, Rotterdam, The Netherlands, under the supervision of Dr. E. A. C. Wiemer and Prof. Dr. G. Stoter.

Table 7

Hydrogen bonding interactions of tributyltin(IV) compounds **1–4** with ribonucleotide reductase (4R1R), thymidylate synthase (2G8D), thymidylate phosphorylase (1BRW) and topoisomerase II (1QZR).

Compound		Amino acids involved in hydrogen bonding			
Compd no.	Groups	4R1R	2G8D	1BRW	1QZR
		Amino acid residue	Amino acid residue	Amino acid residue	Amino acid residue
1	Azo group nitrogen atom(s)	T624–N1 (2.62) T624–N2 (2.92)	R23–N1 (2.94)		
	Carbonyl oxygen atom(s)	E623 (2.31)	R23 (2.75 and 2.82)		
	Hydroxyl group oxygen atom(s)	T209 (2.90), T624 (2.44)	R23 (2.71 and 2.99)	E1022 (2.90)	
2	Sn–oxygen atom(s)		S219 (2.86), H259 (2.97)	Q1064 (2.23)	
	Azo group nitrogen atom(s)	C439–N1 (2.64) C439–N2 (2.07)	R23–N1 (2.96)	R1026–N2 (2.99)	
	Hydroxyl group oxygen atom(s)			Q1064 (2.39)	R77 (2.29)
3	Sn–oxygen atom(s)		R23 (2.98 and 2.64)		
	Azo group nitrogen atom(s)			R1026–N2 (2.97)	
4	Carbonyl oxygen atom(s)	C225 (2.14)		G1066 (2.75), S1065 (2.81)	K102 (2.30)
	Hydroxyl group oxygen atom(s)	Y730 (2.90), C439 (2.47)	H259 (2.85)		
	Azo group nitrogen atom(s)	T209–N1 (2.40)	R23–N2 (2.31)		
4	Carbonyl oxygen atom(s)	S622 (2.37)			S127 (2.96), G143 (2.23)
	Hydroxyl group oxygen atom(s)	R251 (2.56)		E1019 (2.75)	T195 (2.33)
	Sn–oxygen atom(s)		H259 (2.08)		S127 (2.88)

Appendix A. Supplementary data

Crystallographic data (without structure factors) for the structure of **4** have been deposited with the Cambridge Crystallographic Data Centre (CCDC) as supplementary publication no. CCDC 757617. Copies of the data can be obtained free of charge from the CCDC (12 Union Road, Cambridge CB2 1EZ, UK; Tel.: +44-1223-336408; Fax: +44-1223-336003; e-mail: deposit@ccdc.cam.ac.uk; Web site: <http://www.ccdc.cam.ac.uk>).

The following information (Figs. S1–S10) are available as Supplementary Materials. Fig. S1: The structure of $\text{Bu}_3\text{SnL}^2\text{H}$ (**2**) obtained after full geometry optimization; Fig. S2: The structure of $\text{Bu}_3\text{SnL}^3\text{H}$ (**3**) obtained after full geometry optimization; Fig. S3: $\text{Bu}_3\text{SnL}^2\text{H}$ (**2**) docked into the binding site of the enzyme ribonucleotide reductase (4R1R); Fig. S4: $\text{Bu}_3\text{SnL}^2\text{H}$ (**2**) docked into the binding site of the enzyme thymidylate synthase (2G8D); Fig. S5: $\text{Bu}_3\text{SnL}^2\text{H}$ (**2**) docked into the binding site of the enzyme thymidylate phosphorylase (1BRW); Fig. S6: $\text{Bu}_3\text{SnL}^2\text{H}$ (**2**) docked into the binding site of the enzyme topoisomerase II (1QZR); Fig. S7: $\text{Bu}_3\text{SnL}^3\text{H}$ (**3**) docked into the binding site of the enzyme ribonucleotide reductase (4R1R); Fig. S8: $\text{Bu}_3\text{SnL}^3\text{H}$ (**3**) docked into the binding site of the enzyme thymidylate synthase (2G8D); Fig. S9: $\text{Bu}_3\text{SnL}^3\text{H}$ (**3**) docked into the binding site of the enzyme thymidylate phosphorylase (1BRW); Fig. S10: $\text{Bu}_3\text{SnL}^3\text{H}$ (**3**) docked into the binding site of the enzyme topoisomerase II (1QZR). Supplementary data associated with this article can be found, in the online version, at doi: [10.1016/j.jinorgbio.2010.05.001](https://doi.org/10.1016/j.jinorgbio.2010.05.001).

References

- [1] A.S. Abu-Surrah, M. Kettunen, *Curr. Med. Chem.* 13 (2006) 1337–1357.
- [2] K.R. Barnes, S.J. Lippard, *Met. Ions Biol. Syst.* 42 (2004) 143–177.
- [3] V. Cepeda, M.A. Fuertes, J. Castilla, C. Alonso, C. Quevedo, J.M. Perez, *Med. Chem.* 7 (2007) 3–18.
- [4] P. Yang, M. Guo, *Coord. Chem. Rev.* 185–186 (1999) 189–211.
- [5] B. Kelland, *Nat. Rev.* 7 (2007) 573–584.
- [6] P. Kopf-Maier, *Eur. J. Clin. Pharmacol.* 47 (1994) 1–16 and references therein.
- [7] A.Y. Louie, T.J. Meade, *Chem. Rev.* 99 (1999) 2711–2734.
- [8] P.J. Barnard, S.J. Berners-Price, *Coord. Chem. Rev.* 251 (2007) 1889–1902.
- [9] J.D. Robertson, S. Orrenius, *Toxicology* 181–182 (2002) 491–496.
- [10] A.J. Crowe, *Drugs. Fut.* 12 (1987) 255–275.
- [11] M. Gielen (Ed.), *Tin-based Antitumor Drugs*, Springer Verlag, Berlin, 1990.
- [12] M. Gielen, E.R.T. Tiekink (Eds.), *Metallotherapeutic Drug and Metal-based Diagnostic Agents*, Wiley, Chichester, England, 2005.
- [13] S.K. Hadjikakou, N. Hadjiladis, *Coord. Chem. Rev.* 253 (2008) 235–249.
- [14] M. Gielen, M. Biesemans, D. de Vos, R. Willem, *J. Inorg. Biochem.* 79 (2000) 139–145.
- [15] F.P. Pruchnik, M. Banbula, Z. Ciunik, M. Latocha, B. Skop, T. Wilczok, *Inorg. Chim. Acta* 356 (2003) 62–68.
- [16] A. Alama, M. Viale, M. Cilli, C. Bruzzo, F. Novelli, B. Tasso, F. Sparatore, *Invest. New Drugs* 27 (2009) 124–130.
- [17] T.S. Basu Baul, A. Paul, L. Pellerito, M. Scopelliti, P. Singh, P. Verma, D. de Vos, *Investig. New Drugs* (2009) 10.1007/s10637-009-9293-x.
- [18] T.S. Basu Baul, A. Paul, L. Pellerito, M. Scopelliti, P. Singh, P. Verma, A. Duthie, D. de Vos, E.R.T. Tiekink, *Invest. New Drugs* (2009) 10.1007/s10637-009-9360-3.
- [19] R. Willem, I. Verbruggen, M. Gielen, M. Bieseman, B. Mahieu, T.S. Basu Baul, E.R.T. Tiekink, *Organometallics* 17 (1998) 5758–5766.
- [20] T.S. Basu Baul, A. Paul, H.D. Arman, E.R.T. Tiekink, *Acta Crystallogr. E* 64 (2008) o2125.
- [21] M.R. Boyd, Status of the NCI preclinical antitumor drug discovery screen, *Principles and Practice of Oncology*, Lippincott, Philadelphia, vol. 3, 1989, pp. 1–12.
- [22] Y.P. Keepers, P.R. Pizao, G.J. Peters, J.V. Ark-Otte, B. Winograd, H.M. Pinedo, *Eur. J. Cancer* 27 (1991) 897–900.
- [23] C-QSAR Program, BioByte Corp., 201 W. 4th st., Suit 204, Claremont, CA 91711, USA, www.biobyte.com.
- [24] C. Hansch, D. Hoekman, A. Leo, D. Weininger, C.D. Selassie, *Chem. Rev.* 102 (2002) 783–812.
- [25] R.P. Verma, C. Hansch, Development of QSAR models using C-QSAR program: a regression program that has dual databases of over 21,000 QSAR models, *Nat. Protoc.* (2007), doi:10.1038/nprot.2007.125. Freely available at: http://www.natureprotocols.com/2007/03/05/development_of_qsar_models_usi_1.php.
- [26] ACD/PhysChem Suite, 110 Yonge Street, 14th floor, Toronto, Ontario, M5C 1T4, Canada, www.acdlabs.com.
- [27] R.D. Cramer III, J.D. Bunce, D.E. Patterson, I.E. Frank, *Quant. Struct.-Act. Relat.* 7 (1988) 18–25.
- [28] C.A. Bennett, N.L. Franklin, *Statistical Analysis in Chemistry and the Chemical Industry*, John Wiley, New York, 1967, pp. 708–709.
- [29] C.D. Selassie, S. Kapur, R.P. Verma, M. Rosario, *J. Med. Chem.* 48 (2005) 7234–7242.
- [30] A.L. Spek, *Acta Crystallogr. D* 65 (2009) 148–155.
- [31] G.M. Sheldrick, *Acta Crystallogr. A* 64 (2008) 112–122.
- [32] J.J.P. Stewart, *J. Comput. Chem.* 10 (1989) 209–220.
- [33] J.J.P. Stewart, *J. Comput. Chem.* 10 (1989) 221–264.
- [34] J.J.P. Stewart, *J. Comput. Chem.* 12 (1991) 320–341.
- [35] J.J.P. Stewart, *J. Mol. Model.* 10 (2004) 155–164.
- [36] J.J.P. Stewart, *J. Mol. Model.* 13 (2007) 1173–1213.
- [37] J. VandeVondele, M. Krack, F. Mohamed, M. Parrinello, T. Chassaing, J. Hutter, *Comp. Phys. Comm.* 167 (2005) 103–128.
- [38] ArgusLab 4.0.1: Thompson MA, Planaria Software LLC, Seattle, WA, <http://www.arguslab.com>
- [39] Protein Data Bank, <<http://www.rcsb.org/pdb/>>.
- [40] R. Wang, L. Lai, S. Wang, *J. Comput. Aided Mol. Des.* 16 (2002) 11–26.
- [41] T.S. Basu Baul, S. Dhar, N. Kharbani, S.M. Pyke, R. Butcher, F.E. Smith, *Main Group Met. Chem.* 22 (1999) 413–421.
- [42] T.S. Basu Baul, K.S. Singh, A. Lycka, A. Linden, X. Song, A. Zapata, G. Eng, *Appl. Organometal. Chem.* 20 (2006) 788–797.
- [43] T.S. Basu Baul, K.S. Singh, X. Song, A. Zapata, G. Eng, A. Lyčka, A. Linden, *J. Organomet. Chem.* 689 (2004) 4702–4711.
- [44] M. Nádvorník, J. Holeček, K. Handlir, A. Lyčka, *J. Organomet. Chem.* 275 (1984) 43–51.
- [45] A. Lyčka, J. Holeček, M. Nádvorník, K. Handlir, *J. Organomet. Chem.* 280 (1985) 323–329.
- [46] P.J. Harrison, K. Lambert, T.J. King, B. Majee, *J. Chem. Soc., Dalton Trans.* (1983) 363–369.
- [47] T.S. Basu Baul, E.R.T. Tiekink, *Z. Kristallogr. (NCS)* 211 (1996) 489–490.
- [48] T.S. Basu Baul, S. Dhar, S.M. Pyke, E.R.T. Tiekink, E. Rivarola, R. Butcher, F.E. Smith, *J. Organomet. Chem.* 633 (2001) 7–17.
- [49] T.S. Basu Baul, W. Rynjah, E. Rivarola, A. Linden, *J. Organomet. Chem.* 690 (2005) 613–621.
- [50] R. Barbieri, F. Huber, L. Pellerito, G. Ruisi, A. Silvestri, *Chemistry of Tin: ¹¹⁹Sn Mössbauer Studies on Tin Compounds*, in: P.J. Smith (Ed.), Blackie, London, 1998, pp. 496–540.
- [51] R.V. Parish, in: G.J. Long (Ed.), *Mössbauer Spectroscopy Applied to Inorganic Chemistry*, vol. 1, Plenum Press, New York, 1984, pp. 528–544.
- [52] G.M. Bancroft, R.H. Platt, *Adv. Inorg. Chem. Rad.* 15 (1972) 59–258.
- [53] G.M. Bancroft, V.G. Kumar, T.K. Sham, M.G. Clark, *J. Chem. Soc., Dalton Trans.* (1976) 643–654.
- [54] E. Corral, A.C.G. Hotze, H. den Dulk, A. Leczkowska, A. Rodger, M.J. Hannon, J. Reedijk, *J. Biol. Inorg. Chem.* 14 (2009) 439–448.
- [55] A.C.G. Hotze, M. Bacac, A.H. Velders, B.A.J. Jansen, H. Kooijman, A.L. Spek, J.G. Haasnoot, J. Reedijk, *J. Med. Chem.* 46 (2003) 1743–1750.
- [56] C.A. Lipinski, F. Lombardo, B.W. Dominy, P.J. Feeney, *Adv. Drug Delivery Rev.* 23 (1997) 3–25.
- [57] C. Hansch, R.P. Verma, *ChemMedChem* 2 (2007) 1807–1813.
- [58] A. Golbraikh, A. Tropsha, *J. Mol. Graph. Model.* 20 (2002) 269–276.
- [59] A. Tropsha, P. Gramatica, V.K. Gombar, *QSAR Comb. Sci.* 22 (2003) 69–77.
- [60] L. Eriksson, J. Jaworska, A.P. Worth, M.T.D. Cronin, R.M. McDowell, P. Gramatica, *Environ. Health Prospect.* 111 (2003) 1361–1375.
- [61] L. Pogliani, *Chem. Rev.* 100 (2000) 3827–3858.
- [62] S. Wold, L. Eriksson, Statistical validation of QSAR results. Validation tools, chemometrics methods in molecular design, in: H. van de Waterbeemd (Ed.), *Methods and Principles in Medicinal Chemistry*, vol 2, VCH, Weinheim, Germany, 1995, pp. 309–318.
- [63] J.A. Wright, A.K. Chan, B.K. Choy, R.A.R. Hurta, G.A. McClarty, A.Y. Tagger, *Biochem. Cell Biol.* 68 (1990) 1364–1371.
- [64] M. Oblender, U. Carpentieri, *Anticancer Res.* 10 (1990) 123–128.
- [65] G. Nocentini, F. Federici, M. Grifantini, A. Barzi, *Pharmacol. Res.* 25 (1992) 312–313.
- [66] G. Nocentini, A. Barzi, *Biochem. Pharm.* 52 (1996) 65–71.
- [67] G. Nocentini, A. Barzi, *Gen. Pharmacol.* 29 (1997) 701–706.
- [68] D.X. West, A.E. Liberta, S.B. Padhye, R.C. Chikate, P.B. Sonawane, A.S. Kumbhar, R.G. Yerande, *Coord. Chem. Rev.* 123 (1993) 49–71.
- [69] J. Alsner, B.S. Sorensen, V.K. Schmidt, O. Westergaard, *Bone Marrow Transplant.* 12 (1993) S154–S155.
- [70] L.Y. Kuo, A.H. Liu, T.J. Marks, in: A. Sigel, H. Sigel (Eds.), *Metal Ions in Biological Systems*, vol. 33, Marcel Dekker, New York, USA, 1996.